TOOL WEAR MECHANISMS IN TURNING TI-6AL-4V USING TUNGSTEN CARBIDE AND POLYCRYSTALLINE DIAMOND INSERTS

By

David James Schrock

A THESIS

Submitted to
Michigan State University
in partial fulfillment of the requirements
for the degree of

Mechanical Engineering – Master of Science

2013

ABSTRACT

TOOL WEAR MECHANISMS IN TURNING TI-6AL-4V USING TUNGSTEN CARBIDE AND POLYCRYSTALLINE DIAMOND INSERTS

By

David James Schrock

The objective of this work is to identify some of the tool wear mechanisms at the material level for the machining of titanium and to provide some understanding of these mechanisms for use in physics based tool wear models. Turning experiments were conducted at cutting speeds of 61m/min, 91m/min, and 122m/min on Ti-6Al-4V, an alloy of titanium, using two different grades of tungsten carbide cutting inserts and one grade of polycrystalline diamond inserts. Three-dimensional wear data and two-dimensional wear profiles of the rake face were generated using Confocal Laser Scanning Microscopy to quantify the tool wear mechanisms. Additionally, the microstructure of the deformed work material (chip) and un-deformed parent material (work piece) were studied using Orientation Imaging Microscopy (OIM). Observations from tool wear studies on the PCD inserts revealed the presence of two fundamentally different wear mechanisms operating at the different cutting speeds. Microstructural analyses of the chip and the work material showed phase dependent tool wear mechanisms for machining titanium. There is a high likelihood of phase change occurring in the work material during machining, with a transformation from the alpha phase to the beta phase. The observed dramatic increase in wear is attributed to a combination of increased diffusivity in the beta phase of the titanium alloy in conjunction with a higher degree of recrystallization of the prior beta phase upon cooling. Results of other observations such as the influence of carbide grain size on tool wear are also discussed.

The following thesis is dedicated to my loving parents, for sparking the interest of a young engineer

ACKNOWLEDGMENTS

I would like to express gratitude for all of the support that I received in my journey toward the completion of this thesis. First, this thesis would not have been possible without the patient guidance of my advisor, Professor Patrick Kwon, to whom I owe a huge debt of gratitude. I would like to especially thank Professor Tom Bieler in the CHEMS Department, for the countless thought-provoking discussions, the immensely helpful technical expertise, and the invaluable use of his time and research equipment, including but not limited to use of the OIM equipment, chemical prep room equipment, and metallurgical mounting supplies. Other important people who need to be acknowledged include Di Kang for his willingness to help in the acquisition of the EBSD data and Wang Xin for his guidance at the early stages of joining Professor Kwon's machining group, including his expertise in helping to set up the first round of turning experiments. I would like to thank Phil Allen from West Michigan Precision Machining in Grand Rapids, Michigan for his willingness to conduct the titanium turning experiments. I would like to thank my wife for her patience, encouragement, and support over the past three years. Finally, I would like to acknowledge and thank the NSF I/UCRC and the U.S. Army Armament Research, Development and Engineering Center (ARDEC) for granting of financial support of this research.

TABLE OF CONTENTS

LIST OF TABLES

LIST OF FIGURES

KEY TO SYMBOLS

A – yield material constant

B – hardening material constant

C – material constant

d_c – depth of cut in mm

ε_p – equivalent plastic strain

ε_p – plastic strain-rate

ε_{po} – effective plastic strain rate for quasi static reference test

f – feed rate in mm/rev

m – flow softening exponent

n – strain hardening exponent

N.A. – numerical aperture

s – cutting speed in m/min

σ_y – flow stress (Pa)

T – temperature (K)

T_o – reference temperature (K)

T_m – melting temperature (K)

λ – wavelength in nm

z – crater wear depth in nm

z-res – z resolution in nm

INTRODUCTION

1.1 An Overview of Tool Wear in Machining Titanium

After over six decades of research, titanium remains one of the most difficult materials to machine. Excessive tool wear is a major factor in the high cost of producing components from titanium alloys. This expense is prohibitive for many common industrial applications.

The material properties that make titanium alloys desirable for "high tech" structural applications are the same properties that are most responsible for rapid tool wear during machining. In particular, low thermal conductivity, excellent strength properties at high temperature, and high chemical solubility or reactivity of titanium alloys with common cutting tool materials have proven problematic in the selection of a suitable tool material [1] [2] [3]. Hartung and Kramer [3] published a paper in 1982 that compiled a list of common tool materials and ranked their suitability for machining titanium. Over thirty years later, straight grade carbide tools remain the recommended cutting insert for machining titanium due to its combination of wear resistance and low cost (compared to tool materials such as polycrystalline diamond (PCD)) [4].

1.2 Motivation for the Current Work

Many gaps exist in the knowledge of the physics of tool wear in machining titanium. More importantly, the wear mechanisms, which are expected to be quite different from the wear mechanisms in cutting steels, have not been clearly defined [5] [6]. For titanium to gain wider use in industry, significant advancements in cutting tool technology must occur. In particular, a better understanding of the physical and chemical wear mechanisms in machining titanium alloys is needed.

For significant progress to be made, empirical studies need to be replaced by physics based models. This work has attempted to identify favorable characteristics for preventing tool wear at the material level. In addition, the results of this study provided the three dimensional wear data and two dimensional wear profiles that will help in the development of comprehensive physics based wear models for cutting titanium. Only with this understanding, can promising new cutting tool materials be efficiently selected, saving the time and cost associated with empirically based "brute force" methods that have historically been employed by the cutting tool industry.

1.3 The Challenge of Reducing Tool Wear in Machining Titanium

There are many significant challenges impeding the development of satisfactory tool materials for machining titanium. First, the lower thermal conductivity of titanium work material causes higher cutting temperatures than those that occur when cutting ferrous or aluminum alloys [1]. In addition, the maximum temperature and the maximum crater depth occur closer to the cutting edge, and the contact area between the chip and the tool is less than that when cutting iron or steel. Therefore, for equivalent cutting forces, steeper thermal gradients, higher overall temperature nearer to the cutting edge, and higher stress from less contact area lead to a higher probability of catastrophic tool failure from increased chipping of the cutting edge [1]. These factors require an insert used for dry machining of titanium to have good thermal conductivity. Better thermal conductivity decreases maximum temperature, lowers steep temperature gradients, and moves the location of the maximum temperature away from the cutting edge. This reduces the probability of premature fracture from thermal gradient loading.

As a secondary benefit, lower temperatures slow the rate of dissolution, diffusion and chemical reaction of the tool with the titanium work material [1].

1.4 Titanium Tool Wear Theories From the Literature

A thorough review of the literature has provided many different hypotheses that have been developed over the course of the last several decades to describe the mechanisms controlling the wear rate of cemented carbide and polycrystalline diamond (PCD) cutting tools during cutting of titanium alloys. These mechanisms can typically be divided into two catagories: (1) abrasion, attrition or fracture, or (2) diffusion or reaction.

Some authors have identified abrasion or attrition as the major tool wear mechanism in cutting titanium with PCD inserts. König and Neises [7] identified a mechanism by which graphitization of the PCD inserts reduced abrasion resistance of the cutting tool. Corduan et al. [8] attributed crater wear on the rake face of the tool to the formation of a TiC transfer layer that was periodically removed, tearing off tool material with it. Nabhani [9] conducted quasi-static adhesion experiments between titanium and PCD, showing that fracture during separation of the weld point always occurred in the tool for temperatures of 740, 760 and 900°C. In contrast, it was reported that machining tests conducted using PCD at 75m/min showed no evidence of cratering on the rake face.

Other researchers have identified dissolution or diffusion wear as the mechanism controlling the wear rate of PCD inserts during machining of titanium alloys at high speeds. Hartung and Kramer [3] published the result of a series of turning experiments with titanium using various cutting tools. Their experiments identified PCD as the tool with the least amount of wear. From their research, they determined that PCD provided the best wear resistance because it was able to maintain a stable TiC reaction layer on the surface. This reaction layer limited the overall wear rate by reducing the dissolution/diffusion component of tool wear as the tool constituent carbon atoms must transfer through this layer. They did, however, note that the PCD inserts exhibited a scalloped wear pattern on the rake face that was not seen with uncoated carbide inserts. The scalloped wear pattern was attributed to different conditions at the tool-chip interface: areas of sliding, such as areas of chip seizure with no relative sliding.

Min and Youzhen [10] published the results of a tool wear study on milling of Ti-6Al-4V using carbide tools. Tool wear at cutting speeds between 118-235m/min was attributed to the diffusion of carbon and cobalt in regions of chip seizure. The tool and tool/work piece interface was studied using electron probe microanalysis, SEM, wave- length dispersive spectroanalysis, and Auger electron spectroscopy. It was shown that carbon concentration increased near the tool/work interface but decreased in regions of the cutting tool below the surface. Tool embrittlement due to carbon depletion was thought to be responsible for tool failure.

Hua and Shivpuri [4] published a model of cobalt diffusion wear, by which diffusion of the cobalt binder from carbide tools allowed the tungsten carbide (WC) grains to be removed. The results from the model were in reasonable agreement with experimental data.

Schrock et al. [11] recently conducted turning experiments with PCD tools at cutting speeds of 61m/min and 122m/min with a zero degree rake angle. It was found that PCD tools exhibited two different wear types at different cutting speeds. At the lower cutting speed, inserts appeared rough and scalloped on the rake face. At the higher cutting speed, wear produced smoother craters, more characteristic of diffusion/dissolution wear. The wear difference was attributed to the higher thermal conductivity of PCD, and correspondingly lower cutting temperatures, retarding dissolution wear. However, the mechanism for the observed change in wear patterns was not explicitly defined. Development of more accurate, predictive models for crater wear in cutting titanium will require an understanding of how tool wear develops and evolves in machining titanium.

1.5 Characteristics of WC-6%Co and Polycrystalline Diamond (PCD) Inserts

To understand tool wear, the material properties of the tool must first be understood. Two common tool materials used to machine titanium alloys are cemented carbides and polycrystalline diamond. The there a many different cemented carbides, but this work focuses on WC-6%Co, which is a material formed by sintering WC grains in a cobalt (Co) matrix that is 6% of the total by weight.

From a mechanical perspective, there are major differences in the properties of PCD and WC-6Co cutting inserts. First, PCD inserts are much harder than carbide inserts. Typical room temperature hardness for PCD is approximately 6000HK, while typical hardness for fine grained WC-6Co is only 1800HK [6]. On the other hand, transverse rupture strength (TRS) and fracture toughness play an important role in preventing premature fracture. In the case of the WC-6Co (1.45μm average grain size), TRS is approximately 3133MPa with a fracture toughness of 10.18 MPa•$m^{1/2}$ [12]. However, TRS for PCD (2μm grain size, 13% Co) is 1550 MPa with a fracture toughness of 6.86 MPa•$m^{1/2}$ [13]. Therefore, it would be expected that a PCD insert would have superior resistance to abrasion wear due to its higher hardness. However, it would also be expected that a PCD tool would be more susceptible to fracture due to its lower TRS and lower fracture toughness.

Another significant difference is in their thermal properties. PCD has a much higher thermal conductivity than WC-6Co. This difference lowers the rake face temperature for PCD tools, inhibiting dissolution, diffusion, and reaction. Furthermore, lower thermal gradients help to prevent premature failure due to fracture from thermal stresses at the cutting edge.

1.4 Phase Dependent Tool Wear Theory for Machining Titanium

Very little research has been conducted on the effect of phase transformation of titanium on on chip morphology or tool wear. For instance, Shivpuri et al. [14] presented a numerical model that included the effect of phase transformation on chip segmentation. However, the effect of the α-β phase change of Ti-6Al-4V (Ti64) on the changes in crater wear pattern on PCD inserts was not examined. It is possible that this phase change may account for the large variety in reported wear mechanisms of PCD tools used to machine titanium described in the literature. This thesis presents experimental evidence supporting the theory that the phase change in Ti-6Al-4V may account for different crater wear patterns. Specifically, it is proposed that higher cutting speeds lead to higher temperatures during cutting, which increases the relative proportion of beta phase in the Ti work material. This increase in beta phase facilitates the rapid diffusion/dissolution wear observed for speeds of 122m/min using PCD tools and 61m/min or higher using carbide tools. The discussion section provides a brief overview of the different characteristics of the two phases of Ti-6Al-4V, such as deformability and self-diffusivity, and how they affect tool wear.

The following work details a set of turning experiments conducted on Ti-6Al-4V using two grade carbides (fine and coarse grain) and PCD cutting inserts. Three dimensional rake surface measurements were taken for both inserts using Confocal Laser Scanning Microscopy (CLSM). Crater wear profiles were extracted in the direction of the chip flow for the WC-6Co tools and the wear evolution was analyzed. In addition, flank wear for both of the insert materials was measured.

EXPERIMENTAL METHODS AND PROCEDURE

2.1 Titanium Metal Cutting Experiments

Dry turning experiments on Ti-6Al-4V were conducted using two grades of cemented carbide inserts and one grade of polycrystalline diamond inserts. For all cutting tools tested, the base insert geometry was ANSI designation CNMA-432. After being mounted in a Sandvik tool holder, the inserts had a -5 degree lead angle and a -5 degree rake angle with respect to the work material. Lead angle refers to the angle between an imaginary line perpendicular to the direction of feed and a line parallel to the cutting edge of the insert. Rake angle is this context refers to the inclination angle in the tool holder that gives the insert its clearance with respect to the work piece. A feed rate of 0.127mm/rev and a depth of cut of 0.635mm were constant for all tests. A schematic of the test setup detailing the orientation of the tool in the tool holder with respect to the work material can be seen in Figure 1 below.

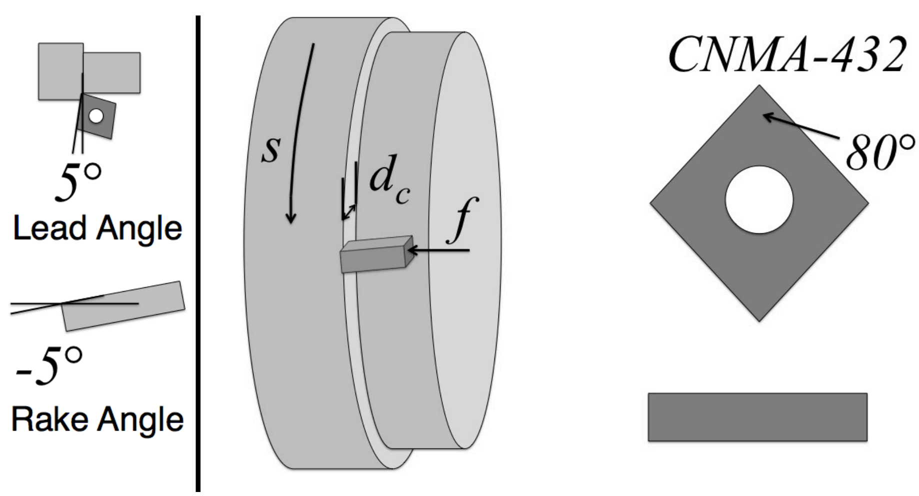

Figure 1 Schematic describing the cutting parameters used in the turning experiments in terms of cutting speed (s), feed rate (*f*), and depth of cut (d_c)

The feed rate was consistent with feed rates used for turning tests on Ti-6Al-4V by various other researchers found in the literature [3] [15]. The depth of cut was chosen conserve work material, while still providing adequate data for wear measurement. Each insert was run for a predetermined time based on an estimated maximum expected tool life for the given cutting speed, and then replaced with a new insert for the successive test. Table 1 below lists the tests cutting tests that were run with the tungsten carbide and PCD inserts.

Table 1: List of the cutting speeds, times, and insert materials used in the machining experiments

	61m/min	**91 m/min**	**122 m/min**
YD101	3 min (chipped) 6 min (chipped) 9 min 12 min	1 min 2 min 3 min (chipped) 4 min	30 sec 1 min (chipped) 2 min (chipped)
YD201	3 min (chipped) 6 min 9 min (chipped) 12 min	All Inserts Chipped	30 sec 1 min (chipped) 2 min
PCD 1200	6 min 12 min 18 min 24 min 30 min (chipped)	No Inserts Tested	1 min (chipped) 2 min 3 min 4 min
PCD 1200 10°	6 min 12 min 24 min	4 min 6 min 8 min	2 min 3 min 4 min

It should be noted that although parameters such as the feed and the lead angle can affect tool life, the objective of this study was to isolate geometry and cutting data from the material characteristics to identify the ability of a tool given material to resist wear. For a fair comparison to be made consistency should be maintained.

Two grades of Zhuzhou Cemented Carbide Cutting Tools, Co, LTD, (ZCCCT, Zhuzhou, Hunan, China) brand uncoated carbide inserts were chosen for the test for their flat rake face. Grade YD201 was a straight grade carbide containing approximately 94% WC and 6% Co. The average grain size was 2μm. Carbide grade YD101 had a composition consisting of 93.6% WC, 0.15%NbC, 0.25%TaC, and 6%Co. The average grain size was 1μm.

The inserts were tested at cutting speeds of 61m/min, 91m/min, and 122m/min. Appropriate cutting data were chosen to differentiate the tests based on cutting temperature. Furthermore, these cutting speeds were chosen because they are in the range where flank wear is stable and crater wear limits the cutting tool life [3]. A set of 10 PCD tools consisted of a Diamond Innovation 1200 grade PCD compact bonded to a tungsten carbide base. The PCD was 92% diamond by volume with an average grain size of 1.5μm. The inserts were tested at cutting speeds of 61m/min and 122m/min [16].

An additional set of turning experiments were conducted on Ti-6Al-4V using PCD tipped inserts with a 10-degree positive rake angle. The PCD tips were Compax® 1200 grade, 92% diamond by volume, with average diamond grain size of 1.5μm manufactured by Diamond Innovation. Shape-Master Tool Company, Kirkland, IL, brazed each PCD tip onto an ISO CNMA120408 carbide base.

Crater wear evolution was studied by machining for successively longer cutting times. After each run, a new corner was used to reduce the possibility of thermal damage from interrupted cutting. At 61m/min cutting speed, three insert corners were used for cutting times of 6min, 12min, and 24min. At 122m/min, three more insert corners were used for cutting times of 2min, 3min, and 4min. Cutting times at 122m/min were shorter than those at 61m/min because the dissolution wear progressed much more rapidly than the attrition wear, resulting in tool failure after only a few minutes of cutting. After each machining test, the tool always had a layer of titanium adhered to the rake surface. In order to study the surface of the PCD tool, the layer was removed by etching in a solution of 48% hydrofluoric acid (HF), 30% aqueous H_2O_2 and water.

2.2 Confocal Microscopy

Crater wear and flank wear were measured in 3-D space using a Ziess LSM 210 Confocal Laser Scanning Microscope (CSLM). Three-dimensional wear topographies were created by generating Maximum Intensity Projection (MIP) images from confocal Z-series that were collected of the rake and flank surfaces of the cutting tools. The MIP images from the microscope were processed using wavelet filtering, following the procedure described by Olortegui-Yume and Kwon [16]. The 3-D surface topographies were graphically rendered in Matlab as a three-dimensional mesh of (X, Y, Z) data from the filtered MIP images. In addition to the meshed 3-D topographies, 2-D wear profiles were also extracted. A combined plot of multiple 2-D wear profiles on the rake face for each cutting time provided quantitative data on crater wear evolution as a function of time. To insure consistency, the 2-D crater wear profiles were taken in a plane parallel to the z-axis along a 45-degree diagonal in the x-y plane. This plane was chosen because it corresponded to the plane that typically exhibited the most crater wear (deepest crater depth) and was in the direction of chip flow. A detailed description of this cross-section is shown below in Figure 2.

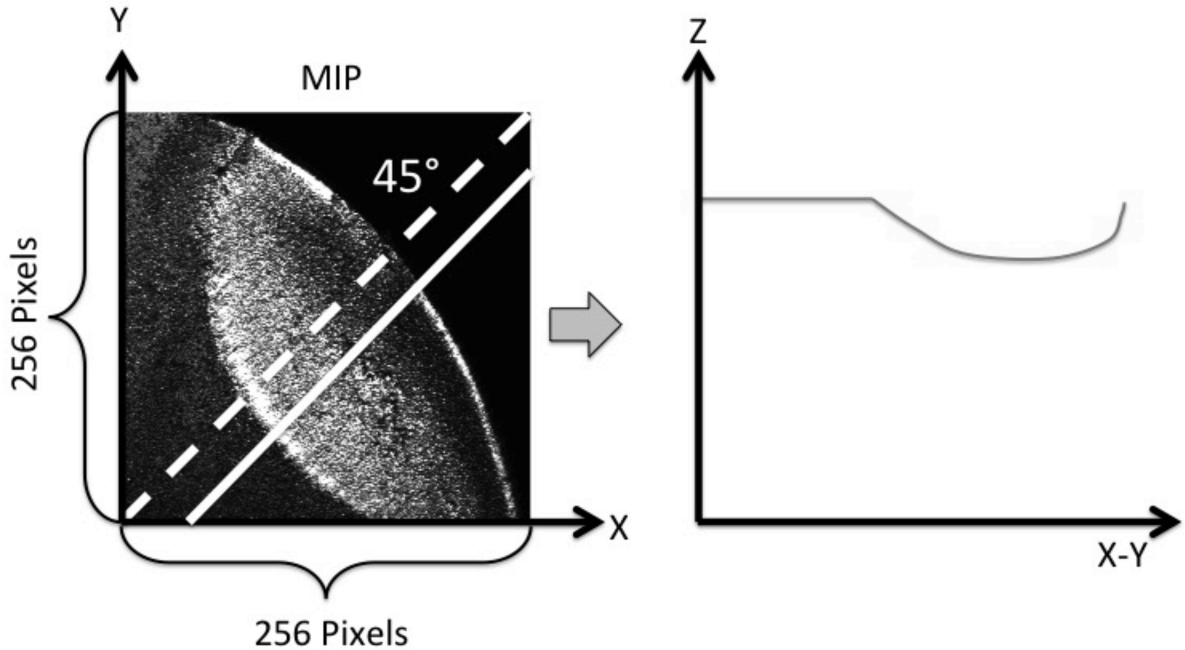

Figure 2: An example of a MIP image from CLSM. The white solid line shows the section at which the crater wear profiles where taken. This cross-section is a plane that is defined by two vectors: (1) a vector parallel to the z-axis and (2) a vector that is 45 degrees from the x-axis in the x-y (shown as the white dashed line) with an intercept of -10 pixels (solid white line). The x and y axis are defined as being along the vertical and horizontal edges of the MIP image in units of pixels.

Various confocal objectives were used in the data collection. Larger objectives typically have a larger numerical aperture (N.A.). Larger numerical apertures and shorter wavelengths of laser light produce finer resolution (smaller value for z_res) in the z-direction. The equation for calculation of the z-resolution of the CLSM is shown below in Equation 1

$$z\_res = \frac{0.62n\lambda}{N.A.^2} \tag{1}$$

where n is the index of refraction of light in air (1.0), λ is the wavelength of laser light, and N.A. is the numerical aperture of the objective.

While it is true that finer z-resolution provides a more precise measurement of wear, the maximum resolution is also limited by the wavelengths of laser light and the objective lenses available on the microscope. Therefore, the shortest available wavelength with the largest objective that still gave a satisfactory field of view was used for the collection of wear images. The laser light used was an argon laser with a wavelength of 488nm. Crater wear on the rake face of the inserts was typically measured using a 20x objective with a numerical aperture (N.A.) of 0.30. Flank wear on the cemented carbide inserts was also measured with this objective. Due the small amount of flank wear typically present on the PCD inserts, a 50x objective with an N.A. of 0.50 was typically used. These combinations provided z resolutions of 3.36μm for the 20x objective and 1.21μm for the 50x objective. Step size for the z-series was then chosen to be something slightly smaller than this z-resolution divided by 2.3, which is consistent with Nyquist theory.

2.3 Orientation Imaging Microscopy

The microstructure of both the as-received work material and the deformed chip was studied using Orientation Imaging Microscopy (OIM). A thin disk of work material with plane-normal parallel to the longitudinal axis of the bar was sliced from the work material using wire Electron Discharge Machining (EDM). Two smaller samples were then cut from this disk also using EDM, which were mounted in metallurgical mount for analysis. The orientation of the samples with respect to the work material is shown below in Figure 3.

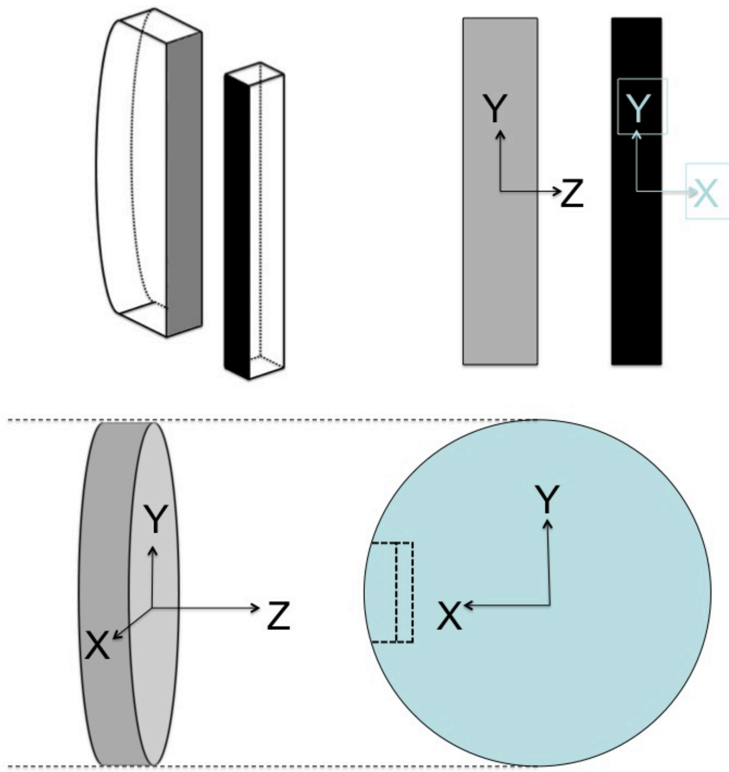

Figure 3: Schematic describing the mounting procedure of the OIM samples in the metallurgical mount. For interpretation of the references to color in this and all other figures, the reader is referred to the electronic version of this thesis.

Wire EDM is commonly used to section metallurgical samples in preparation for mounting, because Wire EDM produces a very small heat affected region that is easily removed during polishing.

Three pieces of a chip from three different conditions were also mounted in a separate metallurgical mount to study the microstructure of the deformed work material. These chips were from cutting the titanium alloy using a PCD insert at speeds of 122m/min, 61m/min and also from cutting using a carbide insert at 61m/min.

The microstructural analyses in this thesis are primarily based upon electron-backscattered diffraction (EBSD), a well-established technique for crystal orientation mapping. In EBSD, an electron beam is focused onto a flat polished sample whose surface normal is tilted 70° from the beam axis. Electrons scattered by the sample in the backward directions form intersecting (Kikuchi) bands on a fluorescent screen (observed by the EBSD camera). These patterns are converted into crystal orientations through a Hough transform [17] [18]. A schematic configuration of EBSD from [18] is shown in Figure 4.

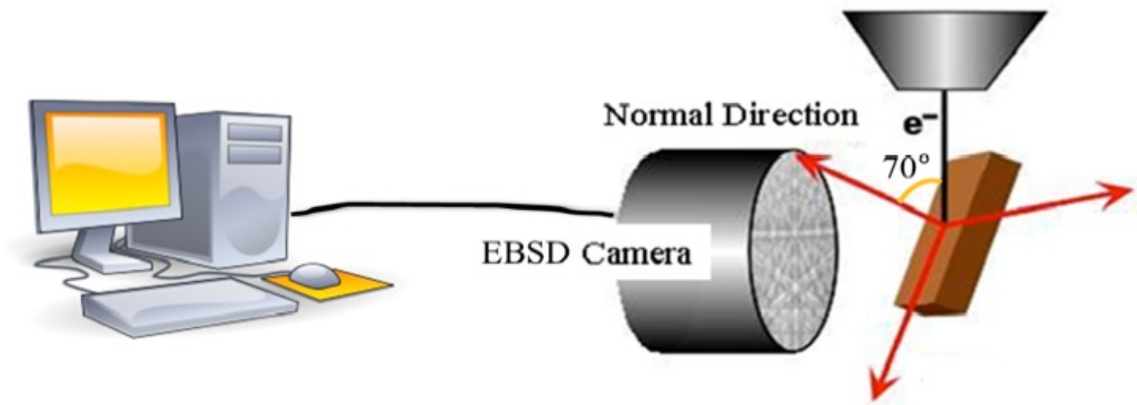

Figure 4: EBSD Setup showing the electron beam, electron backscatter diffraction camera, and the orientation of the sample in the microscope

The EBSD studies were carried out using a CamScan 44 FE scanning electron microscope, with a field emission gun operated at 20 kV using TSL/Link OIM^{TM} system. A working distance of 33 mm was used, and the exposure time for each Kikuchi pattern was 0.08 s. The TSL data collection software was paired with the EBSD camera to instantaneously convert the acquired Kikuchi patterns into crystal orientations. Each crystal orientation thus obtained is recorded as three Euler angles. The step size used for each scan varied and is indicated in the results session. Two steps of cleanup were performed on all the EBSD datasets. The first step was to conduct a neighboring CI (confidence index) correlation procedure, where a data point with a CI smaller than 0.07 (user defined) is reassigned the orientation and CI of its neighbor with the highest CI

[18]. The second step was then to perform a single iteration of grain dilation, using a grain tolerance angle of 5° and a minimum grain size of three pixels.

EXPERIMENTAL RESULTS FOR TOOL WEAR OF WC-6CO INSERTS

3.1 Wear Characteristics of WC-6Co Inserts

As previously mentioned in the introduction, so-called “straight grade” (unalloyed) cemented carbide inserts are considered the current industry standard for machining titanium alloys. Therefore, the two grades of WC-6Co inserts detailed in Section 2.1 were the first set of inserts to be studied in this work. Typical wear patterns on the rake surface of the carbide inserts could be included in one of two categories: either catastrophic failure from chipping of the cutting edge or the presence of a smooth crater, characteristic of either chemical reaction, dissolution, or diffusion of the tool material. Chipping of the insert is considered to be somewhat unpredictable, as it is highly dependent on the individual microstructure of each insert, including but not limited to the presence of pre-existing susceptibility to fracture and fatigue. This work primarily was concerned only with steady state wear, as this type of wear is easier to reliably predict.

A typical example of the type of steady state wear patterns observed on the rake face of the WC-6Co tools is shown in Figure 5 below. Figure 5A shows a MIP image for the carbide insert obtained using CLSM and Figure 5B shows the resulting three dimensional, topographically rendered rake surface. Notice the development of a smooth crater near the cutting edge after machining for 12 minutes at a cutting speed of 61 m/min.

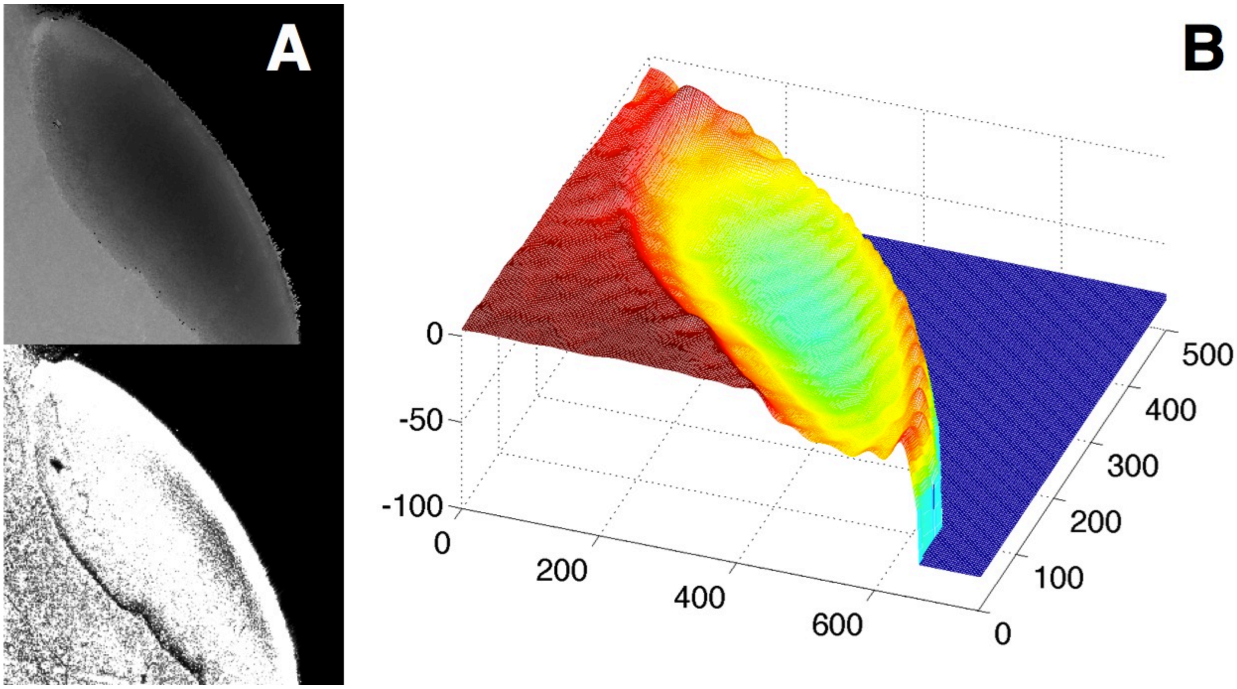

Figure 5: Image A is the MIP collected from the CLSM for the rake face of a YD201 grade WC-6Co insert after machining the Ti6Al4V for 12 minutes at 61m/min. Image B is the 3-D topographical rendered surface.

The individual MIP images and the 3-D surfaces for both grades of WC-6Co inserts, for each cutting time, and for each of the three cutting speeds have been included in Section A1.1 of the Appendix. Once the topographies of the individual inserts were rendered, it was possible to study the 3-D evolution of the crater wear on the rake face of the inserts. The sequence of images in Figure 6 shows how the crater evolves on the surface from a new insert through 12 min of cutting.

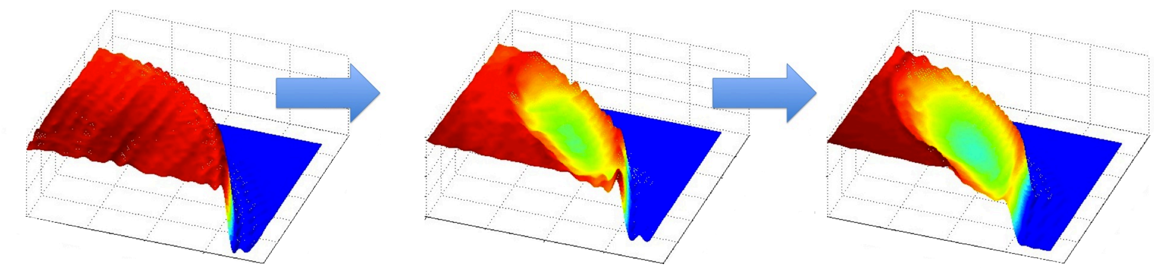

Figure 6: Evolution of crater wear on a YD201 grade WC-6Co insert after machining for 0min, 6min, and 12 min.

After obtaining CLSM results for each insert, crater profiles in the direction of the chip flow were extracted per the method outlined in Section 2.2 and plotted to study crater wear evolution. Figure 7, Figure 8, and Figure 9 compare the crater wear evolution for the carbide tools of grades YD101 and YD201 at cutting speeds of 61m/min, 91m/min, and 122m/min, respectively. From Figure 7 and Figure 9 it is clear that the crater wear is larger for YD101 after 12 minutes of cutting and 30 seconds of cutting, respectively. In addition, it is also clear that the crater wear increases as function of increasing cutting speed. Because cutting speed is the major parameter that determines temperature on the rake surface, the data show the importance of temperature in the wear process.

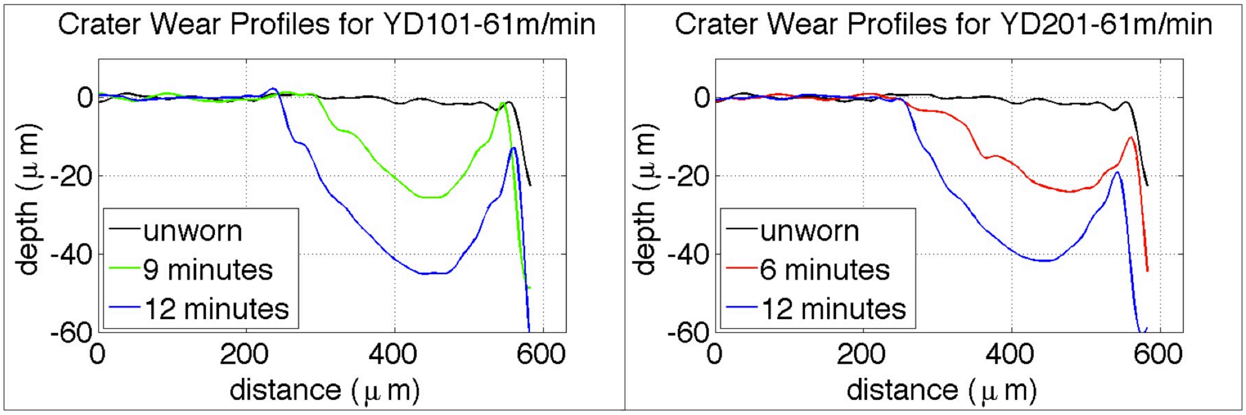

Figure 7: 2-D crater wear profiles from CLSM data showing difference in crater wear evolution for YD101 and YD201 tungsten carbide tools during machining of Ti6Al-4V at 61m/min.

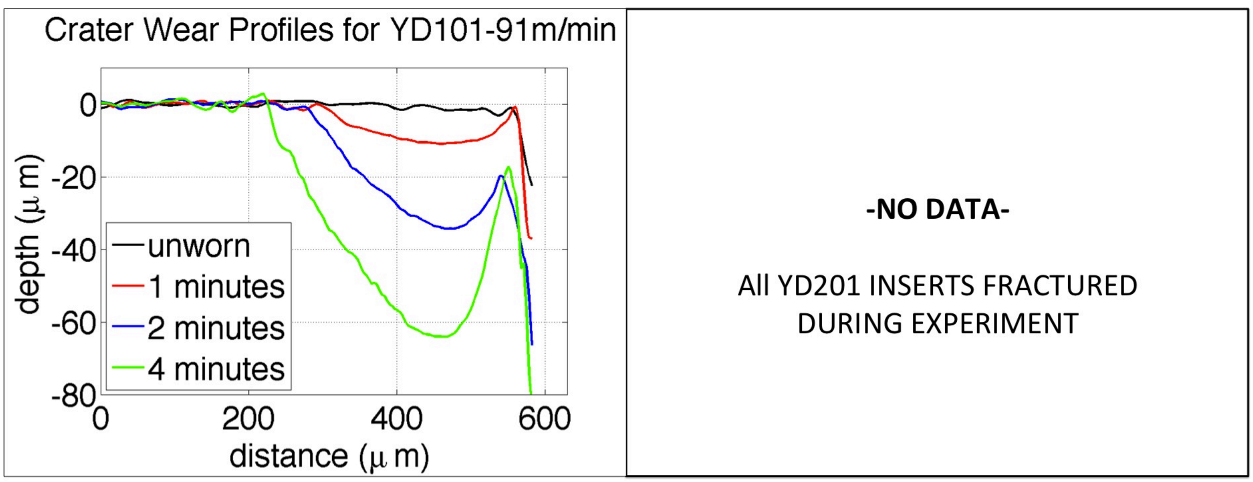

Figure 8: 2-D crater wear profiles from CLSM data showing the crater wear evolution for YD101 grade tungsten carbide tools during machining of Ti-6Al-4V. Note that no steady state wear data was obtained for YD201. All inserts chipped during machining.

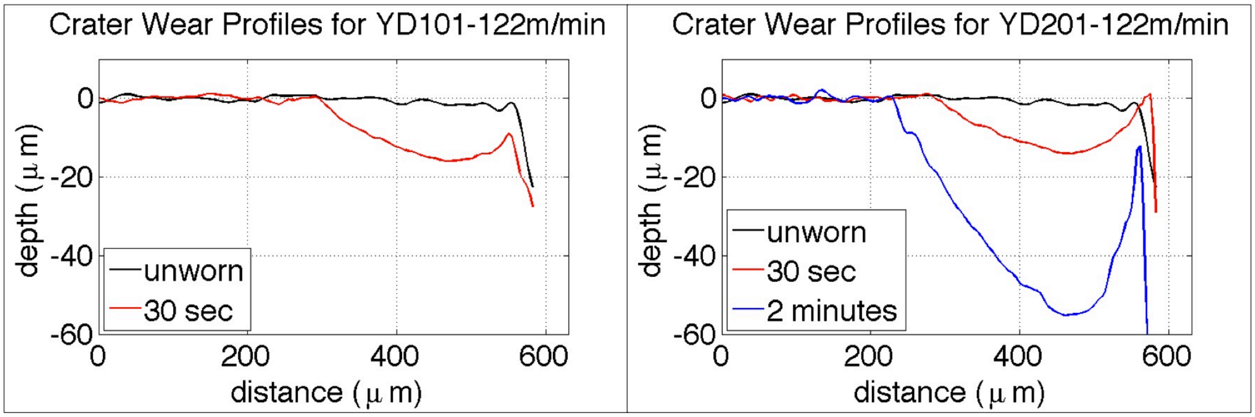

Figure 9: 2-D crater wear profiles from CLSM data showing the difference in crater wear evolution for YD101 and YD201 tungsten carbide tools during machining of Ti-6Al-4V at 122m/min. Note that YD201 shows less wear after 30 seconds of machining.

The wear profiles for YD201 at 300sfm were not presented due to the pronounced fracture. Figure 10 shows the maximum crater depth as a function of cutting time for the two grades of carbide inserts. These maximum values were obtained by taking the maximum 2-D crater depth value from the 2-D wear profiles. This 2-D crater depth corresponds to the maximum 3-D crater depth because the 2-D profiles where chosen to be on the plane that included the maximum crater depth. It should be noted that for the two cutting speeds with data available for comparison, crater depth and hence wear was less for the YD201 grade than for the YD101 grade.

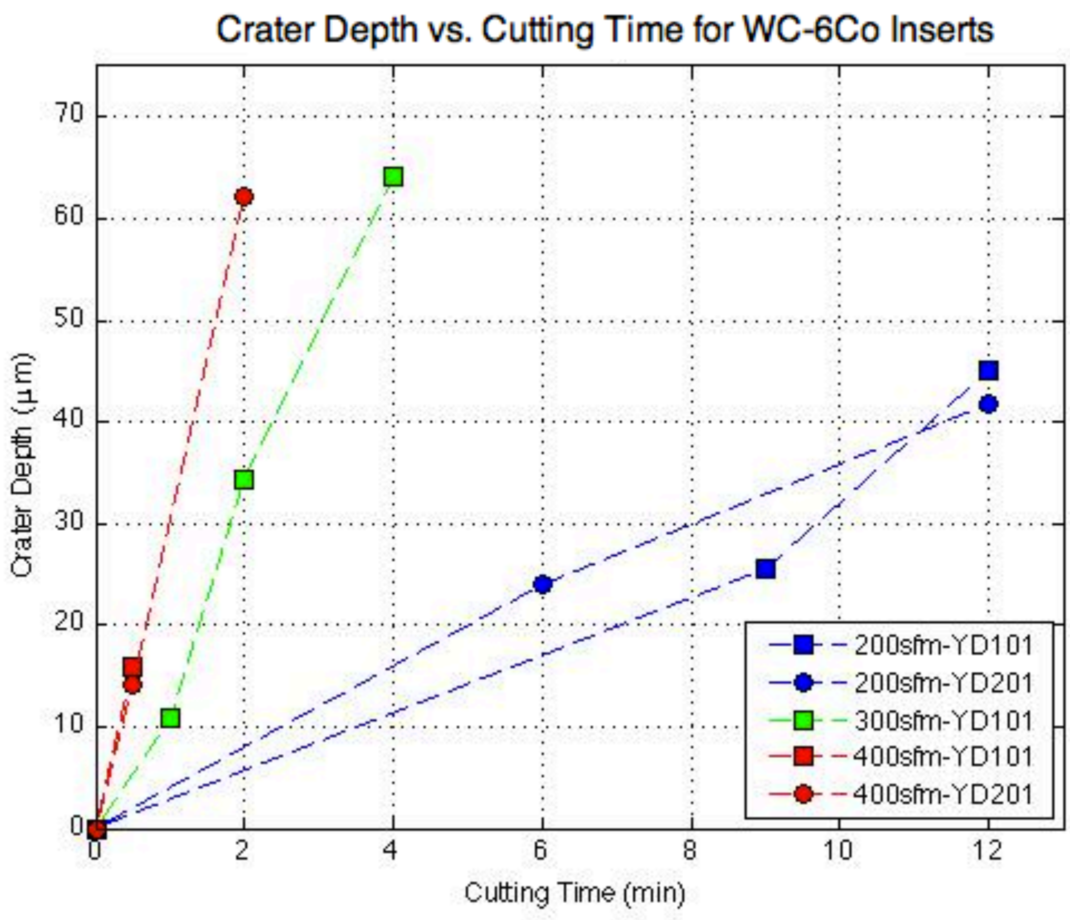

Figure 10: Crater depth versus cutting time for the WC-6Co inserts tested

Flank wear land was also measured and was similarly plotted versus cutting time for the three cutting speeds. The flank wear for both grades can be seen in Figure 11. It can be seen from the wear curves that the YD101 grade of insert exhibited substantially less flank wear land compared to the YD201 grade.

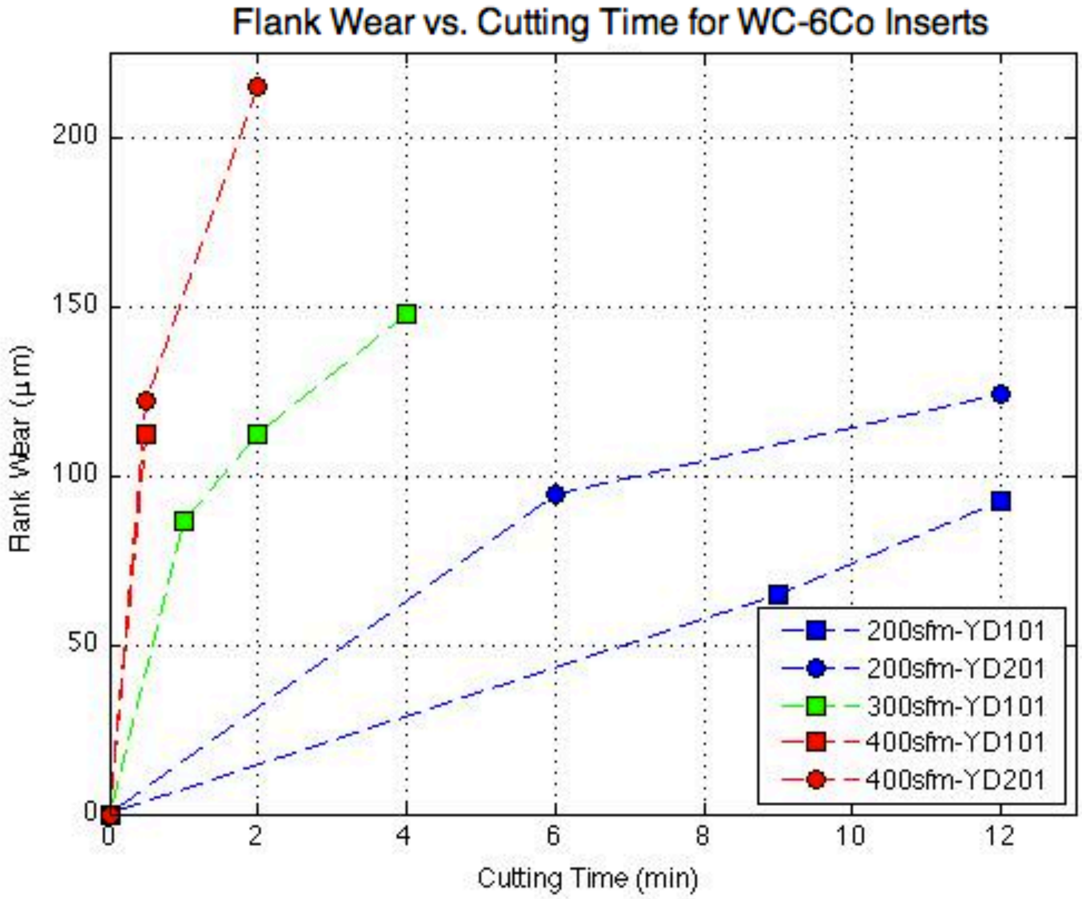

Figure 11: Flank wear versus cutting time for the WC-6Co inserts tested

It was interesting to see that the YD201 grade seemed to be better for reducing crater wear, while the YD101 grade was clearly better at reducing flank wear land. As a final note, while the YD201 grade was consistent in showing a slight reduction in crater wear over the YD101 grade, the difference was within the Z-resolution of the CLSM for the 20x objective used. Therefore, while the consistency of the data demonstrates the possibility of reduced wear for a larger grain sized carbide-cutting insert, it cannot provide definitive proof of reduced wear without further testing with more precise equipment to ensure the validity of the results.

3.2 Wear Characteristics of PCD Inserts

The Polycrystalline Diamond tools were also analyzed using CLSM. The results demonstrated the existence of two distinct wear mechanisms occurring on the rake face of the cutting inserts, which was dependent on cutting speed. Figure 12 shows the wear on the rake face of a PCD insert after machining for 6 min at 61m/min.

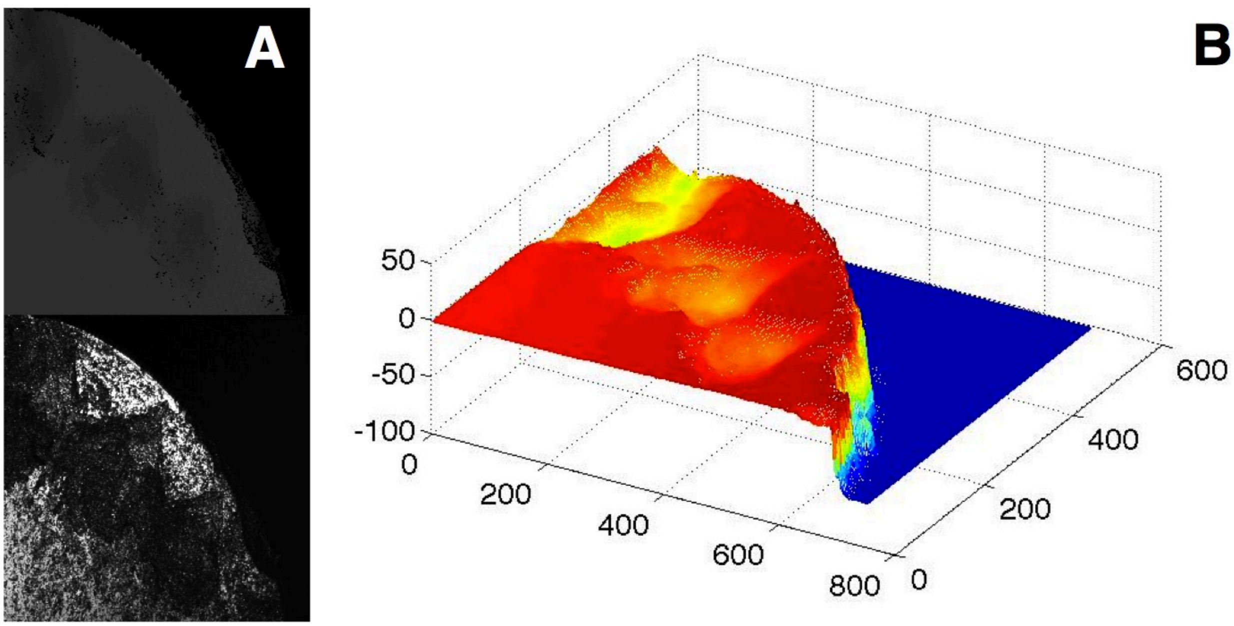

Figure 12: Wear on the rake face of a PCD insert after machining for 6 min at 61m/min

At 61m/min, the tool wear appeared to "scallop" the surface. The wear appeared rough and uneven. The surfaces of the crater were fractured, rather than smoothly worn in the form of a crater.

The wear on the PCD inserts at 122m/min was much different than the wear on the inserts at 61m/min. An example of wear on a PCD insert at 122m/min can be seen in Figure 13below.

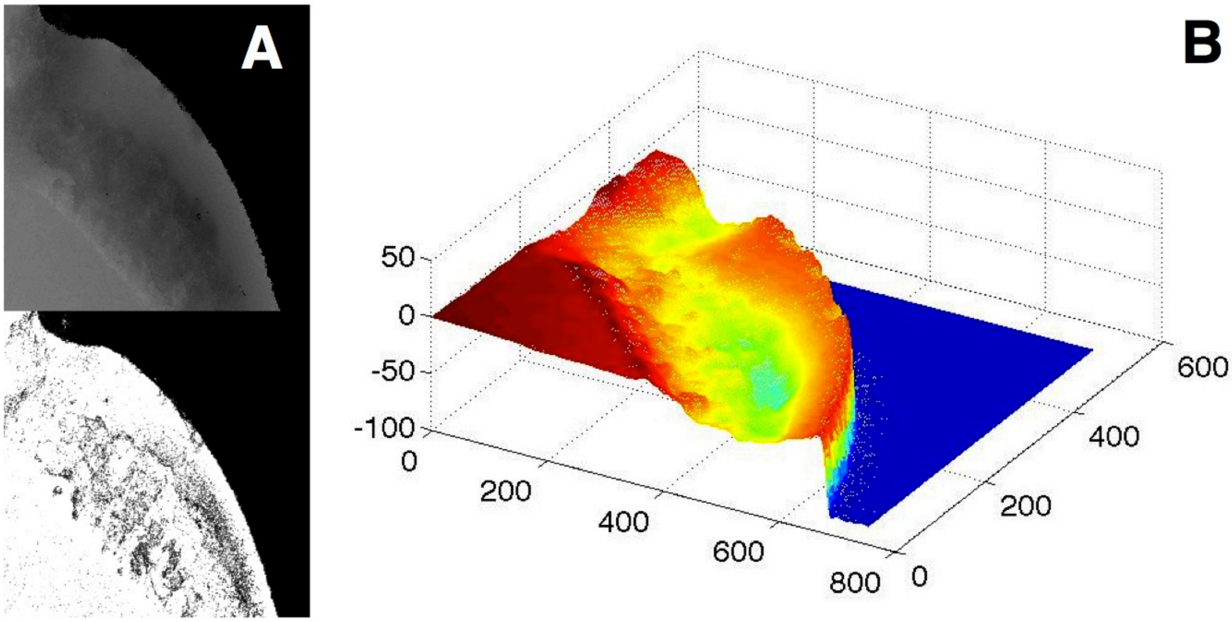

Figure 13: Wear on the rake face of a PCD insert after machining for 3 min at 122m/min

At 122m/min, it is clear that the wear develops into a more conventional, smooth crater. The conventional cratering is indicative of a chemical wear mechanism occurring on the rake surface, such as reaction, diffusion, or dissolution wear. It is notable that the appearance of two different steady state wear patterns, the occurrence of which appeared to be dependent on cutting speed, was unique to the PCD tools. The carbide inserts only exhibited smooth cratering on the surface of the rake face.

3.3 Estimates of Cutting Temperature During Machining of Ti-6Al-4V from FEM

To understand tool wear, particularly both diffusion and dissolution wear, it is necessary to understand the cutting temperature both in terms of magnitude and special gradients. Temperature data is so important because the chemical wear mechanisms such as reaction, diffusion, and dissolution directly depend on the interfacial temperature profile between the tool and work material. In machining, the intimate contact between the cutting edge and the work material causes difficulty for obtaining direct temperature measurements. Thus, finite element simulations have been frequently used, as in this work, to obtain the temperature and traction profiles at the wear surface. The temperature distribution near the cutting edge is of particular interest, because different temperature distributions may create different crater wear patterns. Furthermore, any temperature differences between different cutting tool materials may help to pinpoint the specific wear mechanisms acting on the cutting tool for a given set of cutting data.

In order to understand the observed wear patterns, a Finite Elements Model was used to predict the cutting temperature at the tool chip interface and the special distribution of the temperature gradients in the tool and work materials. Under most Ti6Al4V machining conditions, segmented chip are generated [1] [4] [15]. In our experiment, the chips were in general segmented. However, the finite elements model that was used in this study was limited to machining processes that generate continuous chips. However, since these simulations were only intended to determine temperature, rather than chip morphology, they were deemed to be acceptable for this study. Furthermore, the maximum temperatures obtained in this study were within the range of temperatures obtained experimentally in the literature using tool chip thermocouples [3].

The cutting tools were assumed to be mechanically rigid since deformation of the tool was relatively small but thermally non-rigid with appropriate thermal properties such as heat conductivity and specific heat. The Johnson-Cook (JC) model was used to describe the deformation behavior of Ti6Al4V, and the Arbitrary Lagrangian-Eulerian (ALE) method was used. The equation for the Johnson-Cook flow stress is given in Equation 2 below.

$$\sigma_y(\varepsilon_p, \dot{\varepsilon}_p, T) = \left[A + B(\varepsilon_p)^n\right]\left[1 + C\ln(\dot{\varepsilon}_p^*)\right]\left[1 - (T^*)^m\right] \tag{2}$$

where

$$\dot{\varepsilon}_p^* = \frac{\dot{\varepsilon}_p}{\dot{\varepsilon}_{p0}} \tag{3}$$

and

$$T^* = \frac{(T - T_o)}{(T_m - T_o)} \tag{4}$$

Table 2 lists the Johnson-Cook coefficients of the Ti6Al4V used in many papers [19] [20] [21] [22]. A comparison of models showed little difference in maximum temperature. Therefore, we used Meyer's JC parameter [19] in our simulation. The thermal conductivity of two grades of carbide tools and PCD tools and the simulation results of maximum temperature in the steady state are shown in Table 3. The simulation used a constant friction coefficient of 0.4. Although the friction coefficient is not usually constant for different cutting conditions, it has less impact on temperature, because the majority of heat generated is from plastic deformation.

Table 2: Parameters of Johnson-Cook constitutive model for Ti6Al4V [11]

Reference	A	B	n	C	M
Meyer and Kleponis [19]	896	656	0.5	0.0128	0.8
Lee and Lin [20]	782.7	498.4	0.28	0.028	1.0
Meyer et. al. [21]	862.5	331.2	0.34	0.0120	0.8
Wang et. al. [22]	1165.5	236.6	0.29	0.0355	0.42

Table 3: Estimated temperature during machining from ALE FEM [11]

Grade	Thermal Conductivity W/(m*K)	Cutting Speed (m/min)	Maximum Temperature (°C)
YD101	65	61	1095
YD101	65	122	1198
YD201	75	61	1085
YD201	75	122	1183
PCD	450	61	897
PCD	450	122	991

Figure 14 compares the estimated steady state temperature distribution from FEM for the two different grades of carbide inserts during machining of Ti6Al4V at 61m/min. Results confirm findings from the literature that the maximum temperatures on the tools are higher than those when cutting steel and are much closer to the cutting edge. Furthermore, the steep temperature gradients support the experimental finding of frequent insert failure due to bulk fracture. This bulk fracture was likely due to the high thermal stress from these high temperature gradients.

The small difference in maximum temperature between the two different grades of carbide inserts was surprising. However, this small temperature difference is in agreement with the small difference in maximum crater depth between the two grades of inserts found using CLSM.

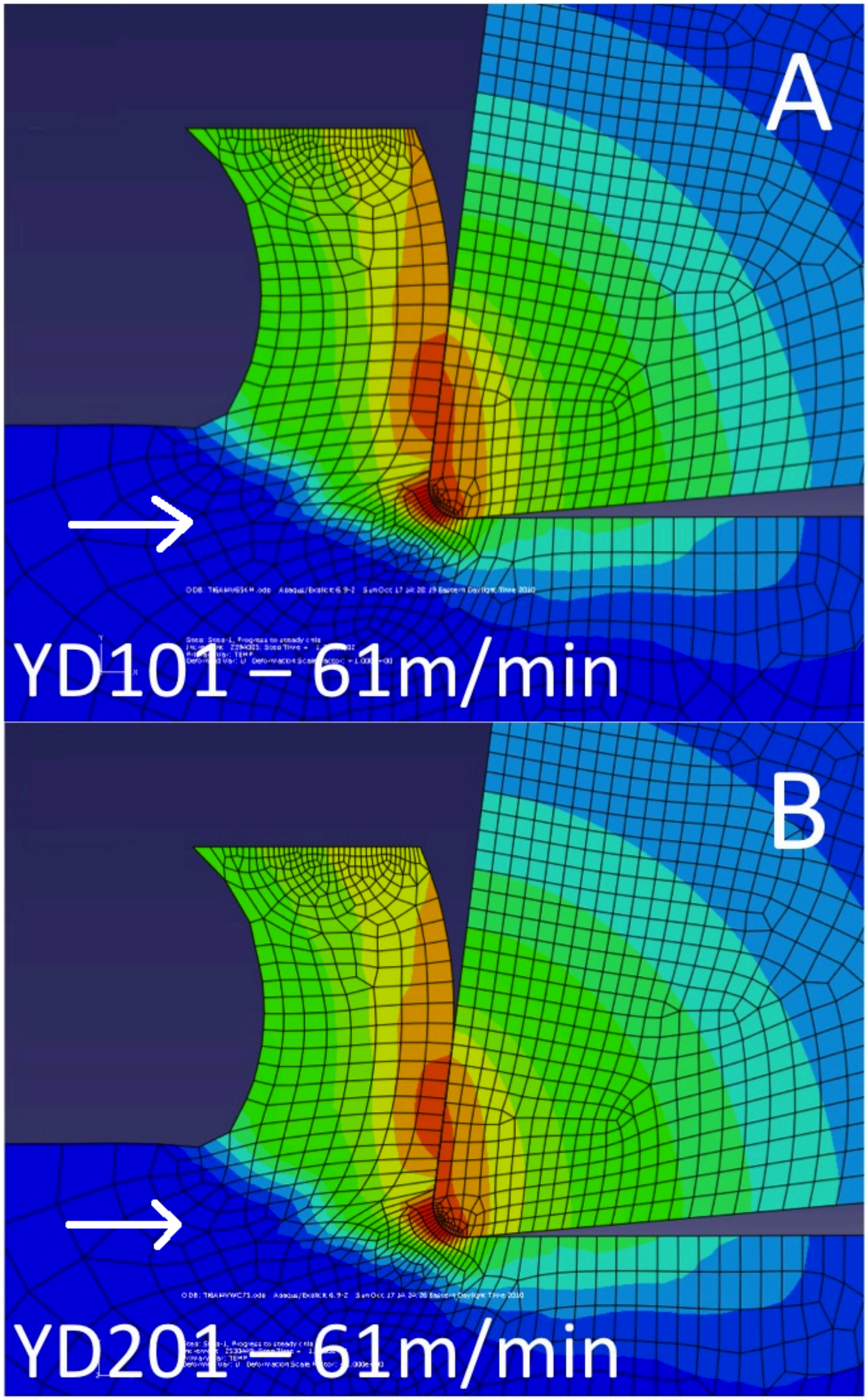

Figure 14: Estimated temperature distribution for carbide inserts at 61m/min

The estimated steady state temperature distribution from FEM for the PCD tools at 61m/min cutting speed is shown Figure 15. As expected, the simulation for the PCD tools predicted lower thermal gradients due to the higher thermal conductivity of PCD compared to WC.

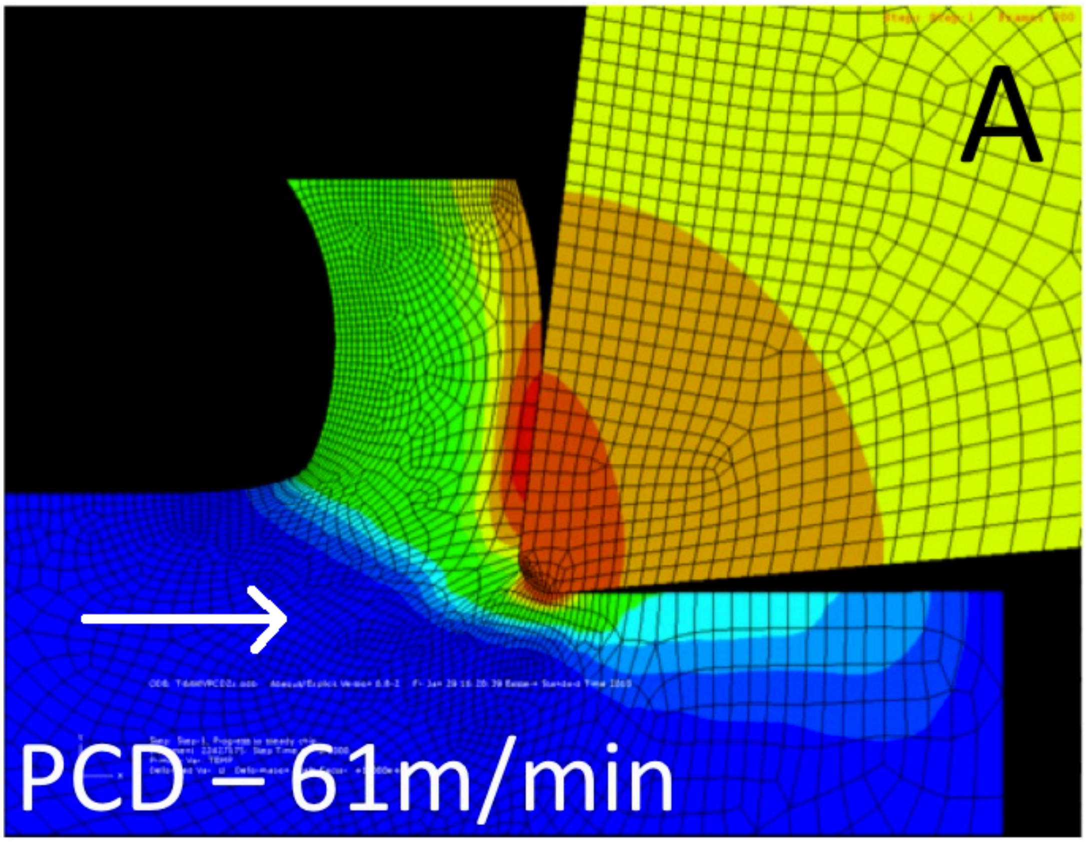

Figure 15: Estimated temperature distribution for PCD inserts cutting Ti6Al4V at 61m/min

3.4 Wear Patterns Indicating Phase Dependent Wear

Figure 16 shows the wear evolution on the rake face of the PCD inserts machining at 61m/min, 91m/min, and 122m/min for the various cutting times indicated.

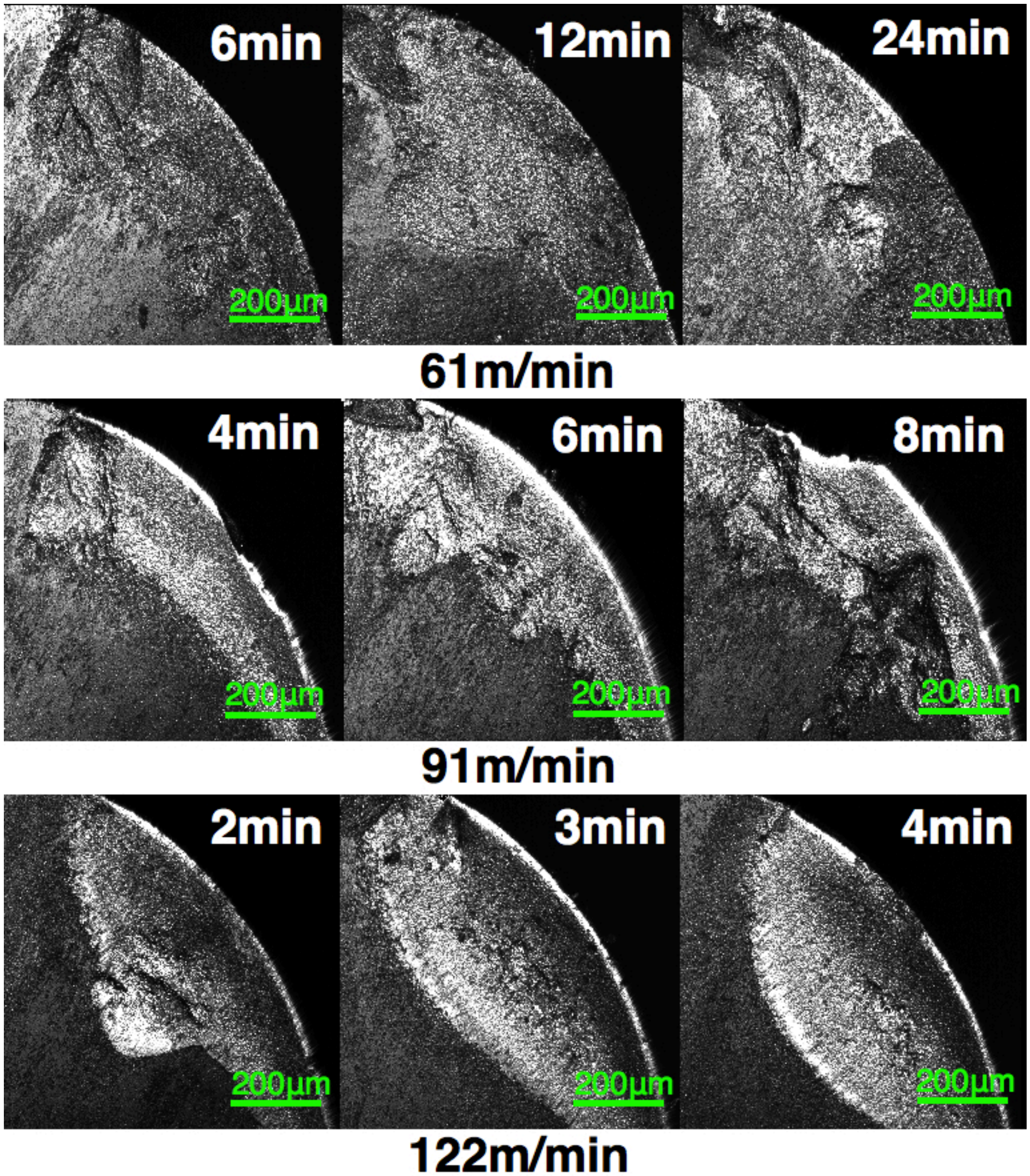

Figure 16: Tool wear on the rake face of PCD cutting tools after cutting at 61m/min, 91m/min, 122m/min. Note the striking difference in wear patterns at each of the cutting speeds.

The images in Figure 16 demonstrate a striking difference in wear pattern on the rake face of the PCD tools at two different cutting speeds. At 61m/min, wear was uneven, fractured, and rough in appearance. Wear appeared similar to that of the adhesion experiments conducted by Nabhani [9]. At the high cutting speed, the wear developed as conventional craters with smooth surfaces characteristic of dissolution wear. Edge stability was relatively good for both cutting speeds, as insert failure from bulk fracture of the cutting edge was rare. The middle row of images in Figure 3 shows the wear evolution on the rake face of the PCD cutting tools at 91m/min. Wear appeared to be a combination of the two distinct wear types observed during machining at 61m/min and 122m/min.

In order to develop a theory of phase dependent wear, the wear on the PCD tools should be compared to wear on other tools. Tool wear of WC-6Co cutting Ti-64 with the same cutting parameters at cutting speeds of 61m/min and 122m/min are shown in Figure 17.

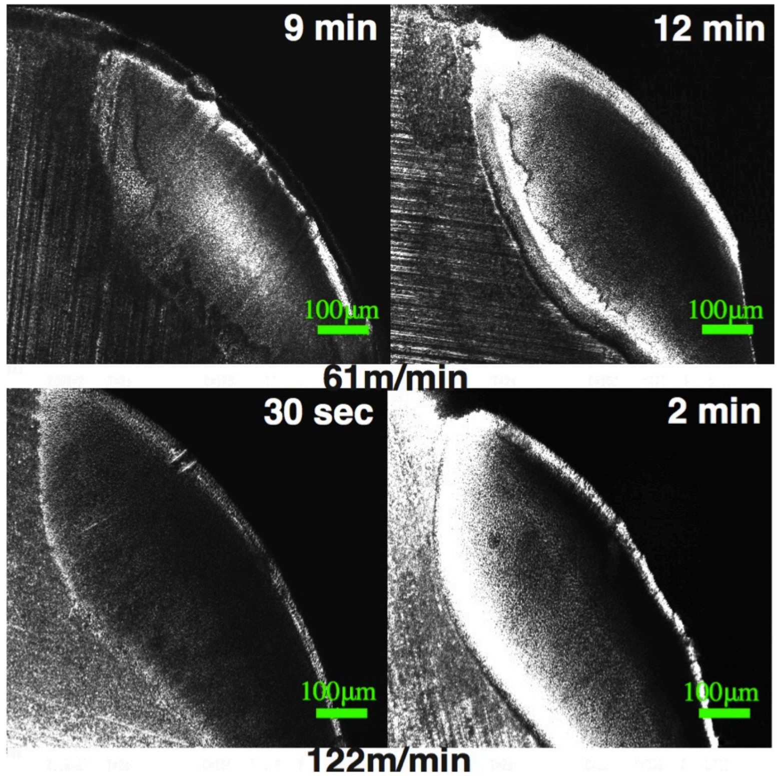

Figure 17: The evolution of wear on the rake face of the WC-6Co after machining at 61m/min (top row) and 122m/min (bottom row) shown at 20x magnification

The effect of the α-β phase change in titanium is evident when comparing the wear observed at the low cutting speed for PCD with the wear observed on the carbide inserts. The carbide inserts at 61m/min did not show the rough, uneven wear seen on the PCD inserts cut at this speed. For WC-6Co tools with the high and low cutting speeds, wear was very smooth showing conventional craters characteristic of dissolution wear.

One significant difference in the PCD inserts was the amount of titanium that remained adhered to the tool after machining. At a cutting speed of 61m/min, little titanium was found on the tools before etching. However, at 122m/min, a significant amount of titanium had adhered. After etching, craters, which are characteristic of dissolution/diffusion wear, were revealed. This can be seen in Figure 18 below.

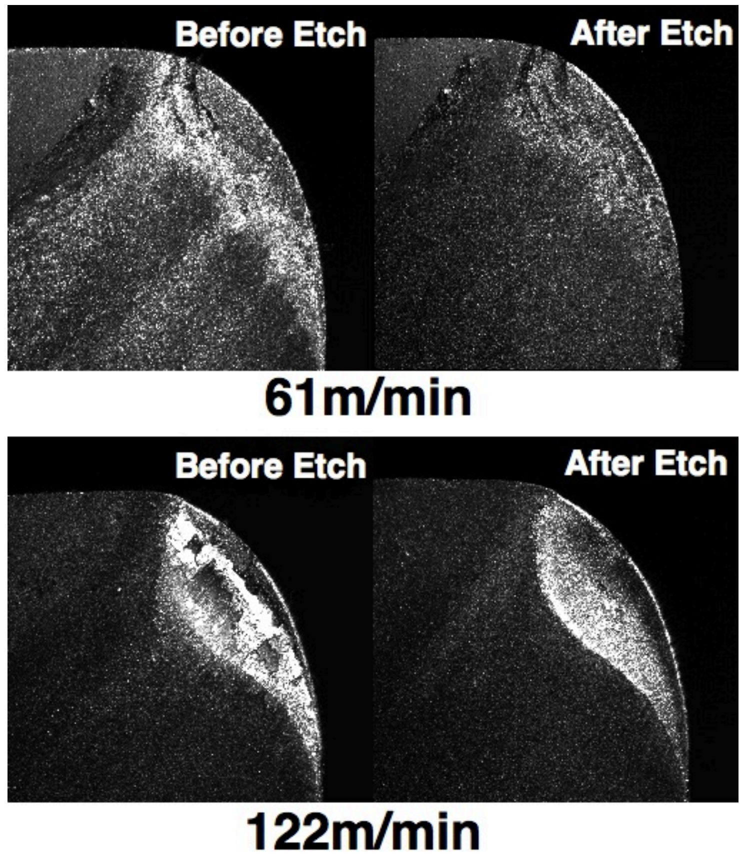

Figure 18: Images showing the rake surface of a typical PCD insert at 10x magnification after machining Ti-64 at 61m/min and 122m/min before and after etching. Note the difference in adhered Ti on the rake face.

3.5 OIM Results

To obtain some understanding of how the microstructure of the work material impacted the tool wear, EBSD patterns were collected of both the as-received work material and the deformed chip following the procedure outlined in Section 2.3. Figure 20 provides an EBSD map of the microstructure of the parent material from a cross-section on the X-Z plane (see Figure 3). The color scheme is based upon -1, -1,1 direction with respect to the TSL coordinate system also described in section 2.3. This plane was assumed to be at ~ 45 degrees from the z-axis of the work material with a shear plane which was assumed to occur at a roughly 45 degree angle from the work piece surface. This shear angle was assumed to be accurate for a small depth of cut and an actual chip thickness roughly equal to the un-deformed chip thickness (feed of 0.127mm) [23]. This map perspective was chosen so the grain orientations would be viewed with respect to the crystal plane that is aligned with the shear plane during chip flow; orientations where shear is imposed on (0001) basal planes are red, and slip directions on prism planes are blue. The relationship between the -1,-1,1 direction in the TSL coordinate system and the shear plane normal in the physical coordinate system is shown in Figure 19 below.

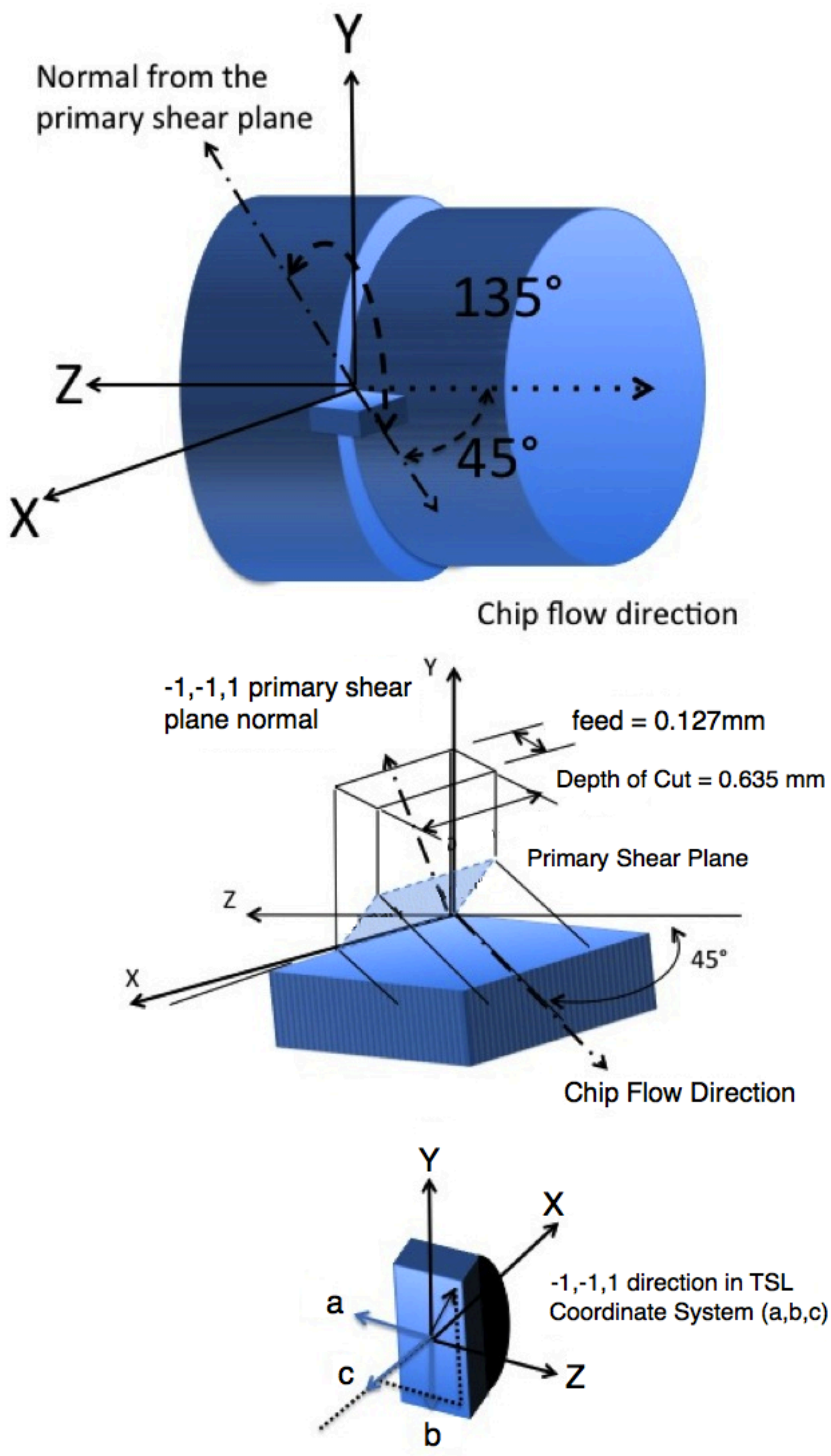

Figure 19: Schematic detailing the relationship between the -1, -1, 1 direction in the TSL coordinate system and the shear plane normal in the physical coordinate system.

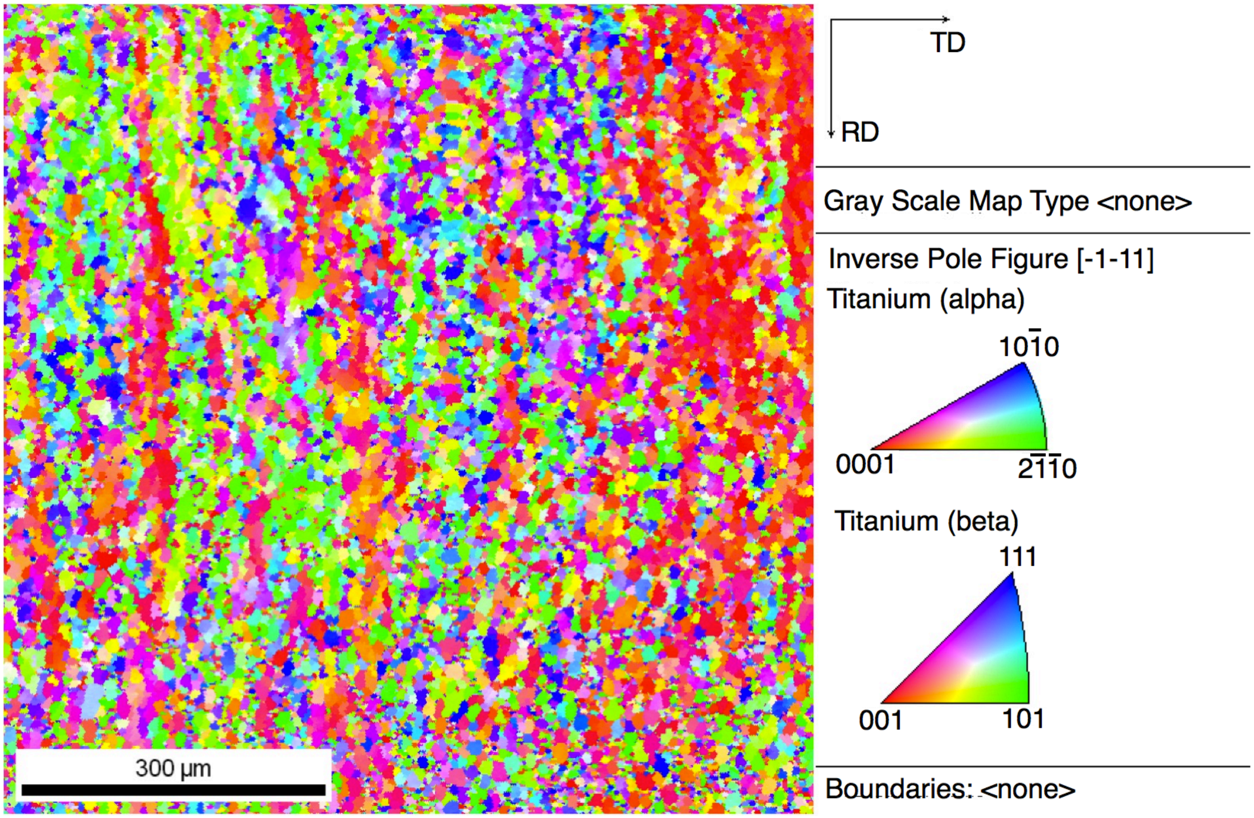

Figure 20: An OIM map of the un-deformed work material on the X-Z plane. The map is viewed from the -1 -1 1 direction with respect to the TLS coordinate system, as detailed in Section 2.3.

Figure 21 is a partition of the microstructure showing only the grains which are oriented with the basal plane within 30 degrees of the -1,-1,1 direction. Shear of these orientations could facilitate a shear transformation from the alpha to the beta phase. The area fraction of the microstructure with this orientation is approximately 16.8% of the total area.

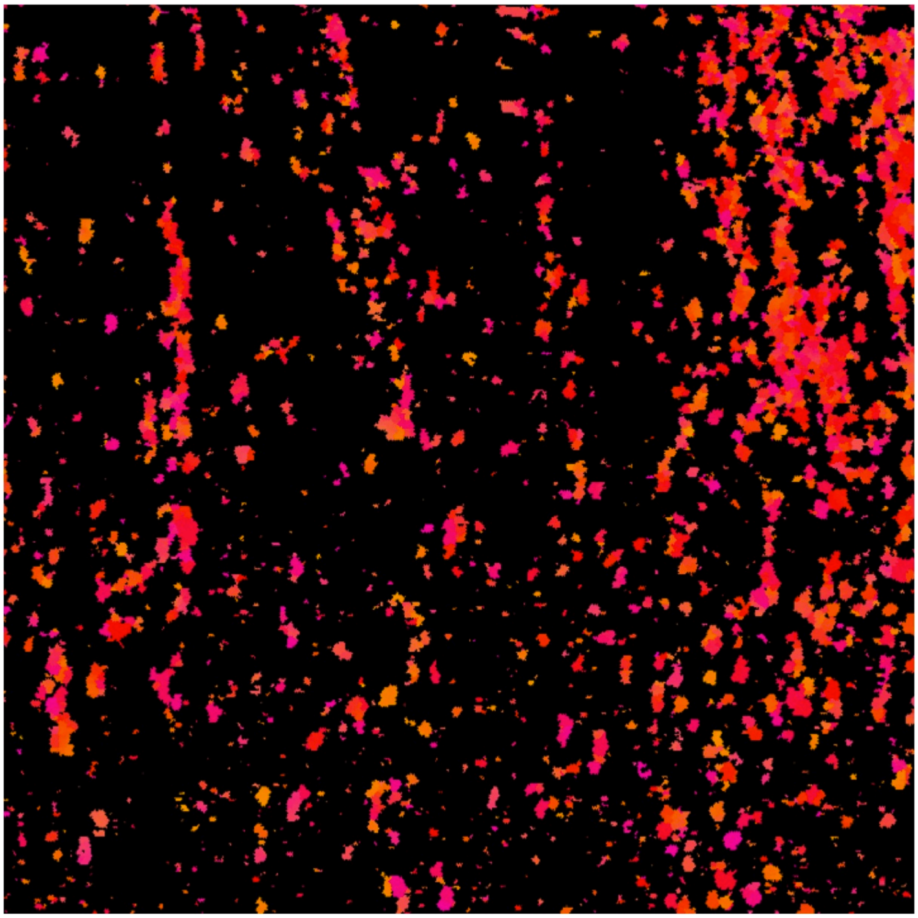

Figure 21: A partition of the OIM map in Figure 20, showing only the regions which are oriented with basal planes within +/- 30 degrees of the -1 -1 1 direction.

The microstructure of the deformed chip was also investigated for evidence of phase change. As with any machining process, the severe deformation of the titanium work material during the chip formation processes causes significant heat generation. However, unlike the machining of other metals such as aluminum or steel, Ti has a relatively low thermal conductivity. This lower thermal conductivity means that the heat built up in the chip is retained and cooling is slow enough that the beta phase formed during machining transforms back into alpha phase. Therefore, the beta microstructure formed during machining cannot be observed directly. Instead, evidence of a phase change from the prior alpha to beta can be observed in the microstructure of the new alpha formed upon cooling of the chip. Figure 22 below shows a representative portion of a chip that was the result of machining using the PCD tools at 122m/min. A plot of misorientation versus distance along the large red arrow in Figure 22 is plotted in Figure 23. This misorientation trace shows several locations where a nearly 90° misorientation across a boundary occurred. This misorientation is a strong indicator, but not a proof of an α-β phase transformation. A 90° misorientation results from α transforming to β {110} plane on the α basal plane, but the reverse transformation occurring on a different 90° misoriented β {110} plane, resulting in a 90° rotation of the α.

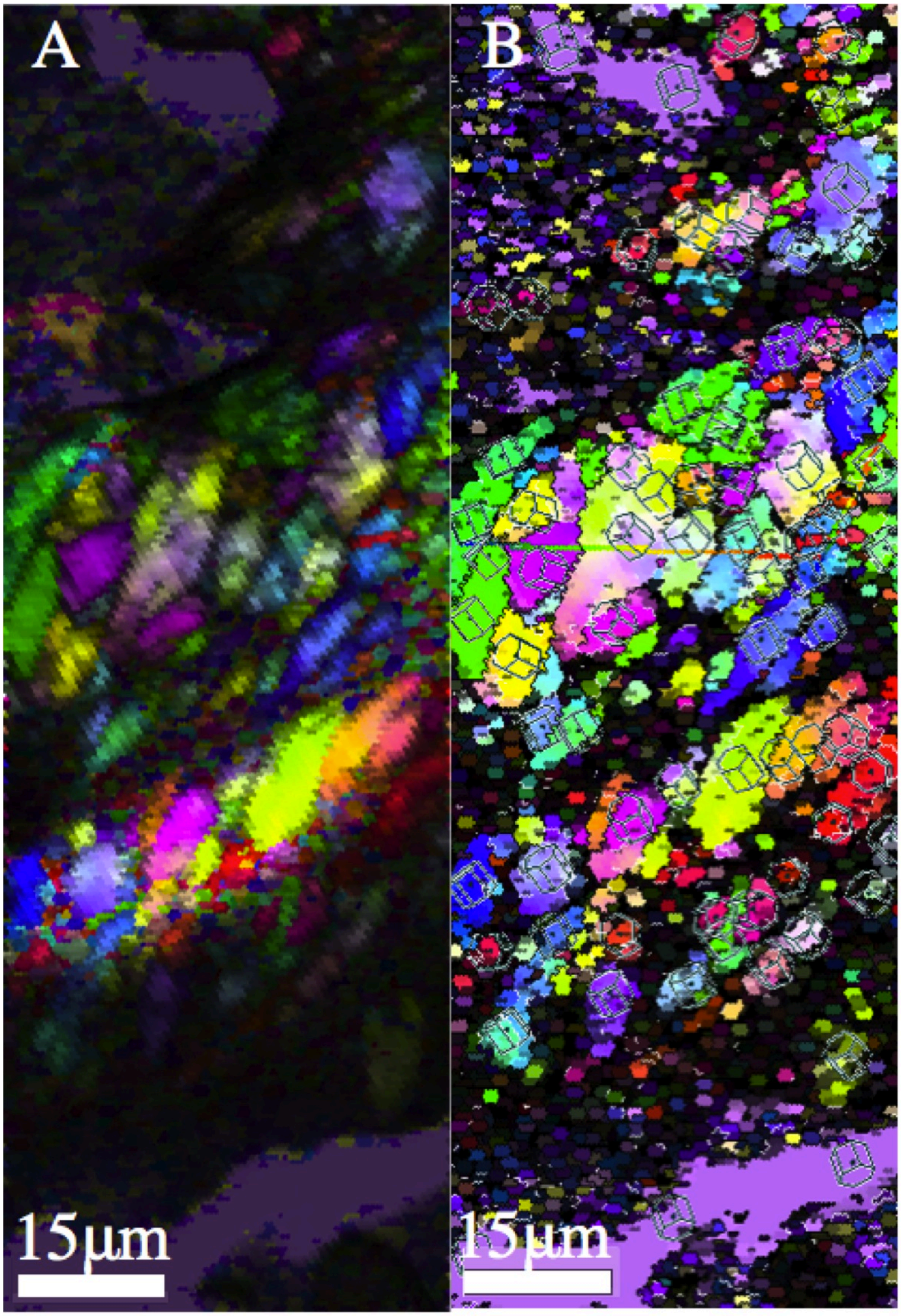

Figure 22: OIM map of the microstructure of the Ti-64 chip after cutting at 122m/min using a PCD insert. The EBSP pattern quality is overlaid in A, while B is the same OIM map showing only the successfully indexed alpha phase.

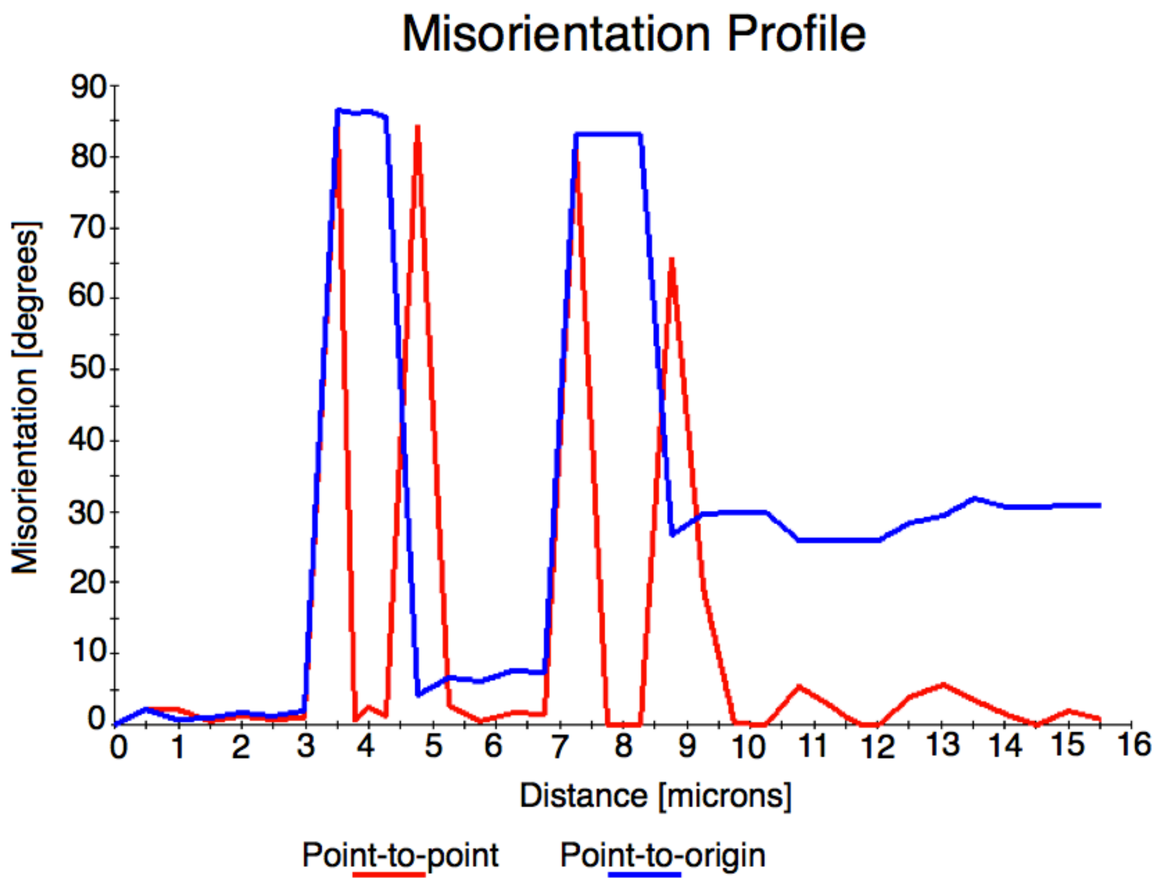

Figure 23: Plot of misorientation versus distance along the line intersecting grains shown in Figure 22

Figure 24 shows the OIM map of a chip after cutting Ti-64 at 61m/min using a PCD tool. Notice how the crystallographic orientations appear relatively uniform, indicated by the constancy of color, particularly between shear bands. This indicates a lower degree of recrystallization of the Ti-64 microstructure.

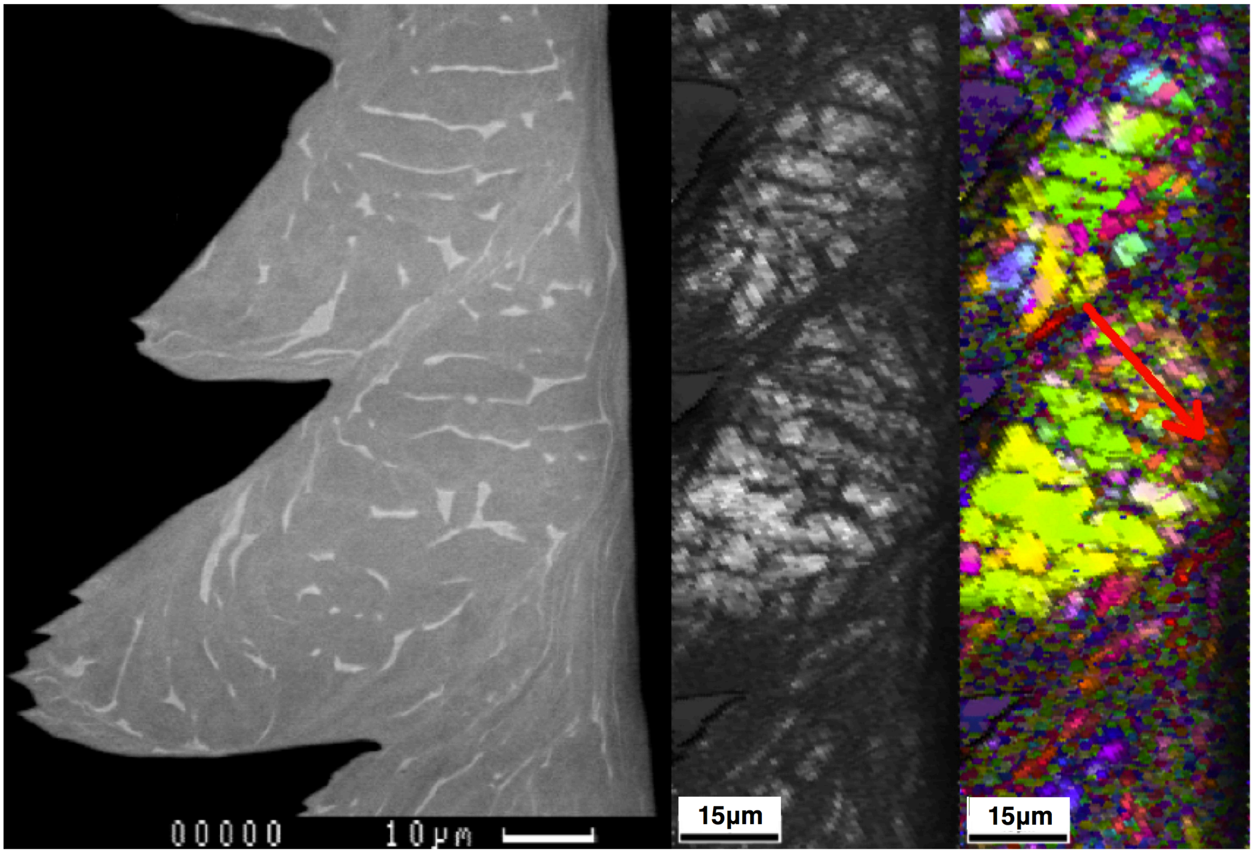

Figure 24: A backscatter image of a section of Ti-64 chip after cutting at 61m/min using a PCD insert with an OIM map of the microstructure. The red arrow indicates the line along which the misorientation profile in was traced.

Figure 25 below shows a smaller portion of the microstructure of the Ti chip shown in Figure 24. The line indicates the direction across grain boundaries for which the misorientation angle was plotted versus distance.

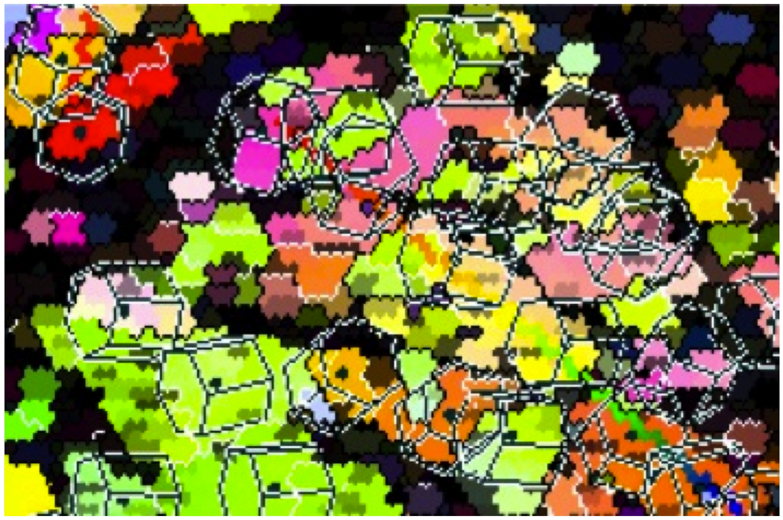

Figure 25: A close up of a portion of the microstructure of the chip in Figure 24 showing the line along which the misorientation profile (Figure 26) was traced.

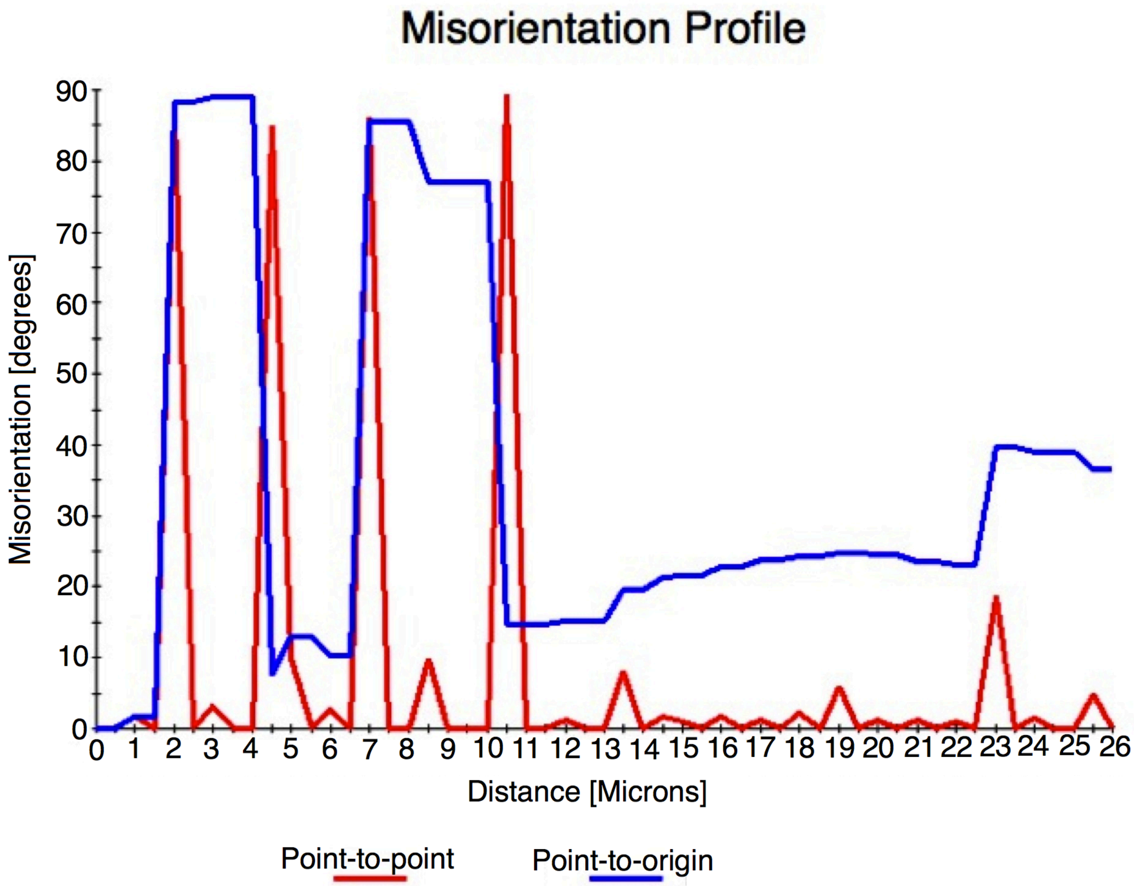

Figure 26: Misorientation versus distance along the line indicated by the arrow in Figure 24. Note the 90-degree oscillating misorientations that strongly suggest phase change in the Ti alloy during chip formation.

DISCUSSION

4.1 The Influence of Cutting Insert Grain Size on the Wear of WC-6Co Inserts

As expected, crater wear developed on the rake faces of the WC-6Co inserts. Once the layer of titanium adhered to the tool had been removed, the surfaces of the craters were very smooth, indicative of dissolution/diffusion wear.

From a comparison of the crater wear profiles, YD201 grade performed slightly better than the YD101 grade. After machining for 12 minutes at 61m/min with YD101 grade insert, crater depth reached a maximum of around 45µm. This compared to a depth of only 42µm using the YD201 grade under equivalent testing parameters and cutting time. A similar result could be seen at a cutting speed of 122m/min for 30 seconds, with crater depths of 26µm and 24µm for YD101 and YD201, respectively.

One possible explanation of the results obtained has already been reported in the literature. In summarizing the work of Freeman et al., Machado et. al. [1] reported that steel-cutting grades of WC/Co containing additives such as TaC are more susceptible to both attrition wear and diffusion wear than straight grade carbides. Dearnley and Grearson [15] also noted the unsuitability of steel-cutting grades of carbide, after obtaining similar experimental results. It should be noted, however, that the relative amount of additives is very small. Typical steel cutting grades of WC/Co replace between 10-25% of their WC with TaC, the YD101 grade only contained 0.25% TaC.

A second possible explanation may help to explain the superior performance of the YD201 grade for resisting crater wear. The main difference between the two grades of inserts was a difference in grain size. A hypothesis was developed, stating that the difference in grain size may have resulted in a difference in rake face temperature. The temperature difference could be explained by the difference in thermal conductivity between the two grades of carbide inserts. As dissolution/diffusion are thermally driven processes, any difference in steady state temperature would have played a role in crater wear rate.

A review of the literature supports this hypothesis. For instance, Frandsen [24] conducted extensive testing on the thermal conductivity of carbides. His research found that the thermal conductivity increased as grain size increased in WC-6Co. Frandsen [24] attributed this increase to increased grain contiguity and decreased phonon scattering at the grain boundaries. This research supports the decreased wear rate of the larger grained YD201 grade.

The increase in thermal conductivity is particularly important at higher cutting speeds, as rake face temperature differences become even greater. Increased temperature on the rake face results in accelerated crater wear. FEA confirmed this hypothesis. For a cutting speed of 61m/min, the temperature difference between the two carbide grades was approximately 10°C. At 122m/min, the temperature the difference between the two grades was around 15°C.

Other interesting observations were made from the results of the CLSM data and the FEA simulations. For instance, an estimated range of distances from the location of the maximum crater wear to the cutting edge was made. From the experimental results, it appeared that the maximum crater depth occurred about 75μm from the cutting edge at 200sfm. However, FEA simulations placed the maximum temperature, and therefore the expected maximum crater depth, about 24μm from the cutting edge, nearly 3 times closer than experimental results. This indicates that the location of maximum crater depth is influenced by more than spatial distribution of cutting temperature. For instance, the location of the maximum crater depth is likely influenced by of the concentration gradients of the tool constituents and the work material, as expected from Fick's Laws of diffusion.

Results from an analysis of the flank wear data indicate that decreasing grain size in WC-6Co reduces flank wear. Mechanical properties of WC-6Co provide an explanation of this phenomenon. Hardness of WC-6Co increases as a function of decreasing grain size [6]. The increase in hardness of the finer grained carbide tools reduces abrasion, one of the main mechanisms of flank wear.

It should be noted that thermal conductivity may play a smaller role in the machining of Ti-64 in conjunction with a cutting fluid, as the coolant will decrease the temperature gradients, resulting in wear mechanisms that are controlled more by abrasion and adhesion. When using a cutting fluid, it may be more beneficial to select harder, finer grained WC-Co to reduce abrasive wear on the flank and increase edge stability.

It should be noted that this study only provides two data points for direct comparison, which means that the statistical significance of the results cannot be confirmed. Furthermore, the observed difference in crater depth is near the theoretical z resolution of the microscope for the combination of N.A. and wavelength of laser light used. This means that there is a potential for measurement error to influence the results. Therefore, more experiments should be conducted with more precise equipment and a larger sample size to increase the confidence in these results.

4.2 Phase Dependent Tool Wear

Overall, the PCD tools performed much better than the WC-6Co inserts. The cutting times at both the high and low cutting speeds far exceeded what was possible with the carbide inserts. In addition, the PCD had better edge stability than WC-6Co. This was likely the result of lower temperature gradients from the higher thermal conductivity. Furthermore, the higher hardness helped to prevent plastic deformation of the cutting edge.

Unlike the carbide tools, dissolution/diffusion crater wear did not appear to be the dominant wear mechanism for PCD at the lower cutting speed. The difference in wear between the two insert materials could be also attributed to the much higher thermal conductivity of PCD. At 61m/min, the wear on the PCD tool was more characteristic of adhesive wear. Adhesion is a wear mechanism that typically occurs at temperatures below those at which diffusion wear predominates. Adhesion wear occurs during high contact pressures and temperatures, where the two metals bond together [6]. When the adhered material breaks loose, it often fractures off tool material with it, generating the observed wear[6] [9]. The PCD tool was much more susceptible to adhesive wear because its lower TRS and lower bulk fracture toughness compared to cemented carbide allows cracks to propagate more easily during the periodic separation of the weld. The scalloped nature of the wear seen in Figure 12 supports this hypothesis.

At higher cutting speeds, the crater wear tended to suggest a diffusion/dissolution dominant wear mechanism. Figure 13 shows the crater of a PCD tool after 3 minutes at 122m/min. Note that a more conventional crater has replaced the scalloped wear pattern. Adhesive force on the PCD insert still created the uneven wear not seen in the carbide craters.

Therefore, the crater wear on PCD inserts is a simultaneous combination of two different wear mechanisms, the relative magnitude of which is determined by the cutting temperature and other phenomena such as the phase of the work material. Adhesive wear, in conjunction with conventional dissolution and diffusion wear can occur on PCD tools in the range of cutting speeds tested.

The dramatic contrasts in wear types seen on the PCD tools in Figure 16 indicated the likelihood of two fundamentally different wear mechanisms operating at the different cutting speeds. In addition, comparison of Figure 16 and Figure 17 shows the disparity in wear pattern between WC-6Co and PCD at low cutting speed. It is important to note that cutting speed has a strong influence on temperature on the rake face. Therefore, the approximately 200°C difference in temperature between the carbide and the PCD tools, obtained from FEM, is thought to be one of the likely causes of the difference in observed wear mechanism.

At the low cutting speed of 61m/min, wear on the rake surface was rough and discontinuous. No diffusion/dissolution wear was observed on the inserts. This type of wear has been referred to as attrition wear [23] in the literature. It is typically produced at lower temperatures by an adhered layer periodically breaking off the surface of the tool, removing relatively large fragments of tool material, microscopic in size [23]. Wear due to diffusion is typically negligible when such relative sliding at the chip-tool interface occurs [3]. The lack of adhered material remaining on the surface after machining but before etching seen in Figure 18 (top) provides experimental support for the hypothesis that relative sliding occurred when machining at 61m/min, inhibiting diffusion wear.

Conversely, the wear on the rake face at the high cutting speed of 122m/min was very smooth in nature, characteristic of diffusion/dissolution wear. The wear in this case likely occurs in a manner similar to the reaction-diffusion mechanism claimed by Hartung and Kramer [3]. The generation of smooth craters implies chip seizure and the presence of a flow zone [3]. The lack of relative motion between the chip and the tool prevents abrasion, which would generate a rough wear surface. A flow zone requires the chip flow to be due to internal shear within the chip itself (convective motion near the chip-tool boundary). The large amount of adhered titanium that remains on the tool before etching seen in Figure 18 (bottom) provides experimental support for the evidence of a flow zone during cutting at 122m/min.

As cutting speed was the independent variable in the experiment, a relatively reliable estimate of temperature in connection with cutting speed was needed to understand its impact on the disparity in wear pattern. FEM simulations previously conducted [11] indicated that the cutting temperature on PCD tools machining Ti-64 at 61m/min with same feed rate and depth of cut was approximately 897° C. Temperature at 122m/min was estimated at approximately 991°C. Table 1 summarizes the results from FEM simulations exhibiting the difference in cutting temperature between PCD and WC-6Co tools. Although the approximately 100°C difference in temperature between the cutting tools is one of the factors affecting the diffusion rate of constituent atoms in the chip, there are likely other physical mechanisms, particularly at the microstructural level, that are controlling the rate of diffusion wear. Furthermore, it is surprising that at 800°C, no smooth cratering was observed. One significant microstructural effect that is likely influencing the diffusion wear rate is a phase change of the work material during cutting.

In order to understand any potential for phase change during machining, the microstructure of Ti-64 is briefly reviewed. Ti-6Al-4V is a two-phase alloy of alpha (hexagonal (HCP) structure) and beta (body-centered cubic (BCC) structure) [1] [25]. As the temperature increases, the fraction of alpha phase decreases, transforming into beta phase. Between 950°C and 1000°C the transformation is complete, and the alloy is completely in the beta phase. The phase diagram modified from Leyens and Manfred [25] in Figure 27 below shows the Ti-6Al- V system.

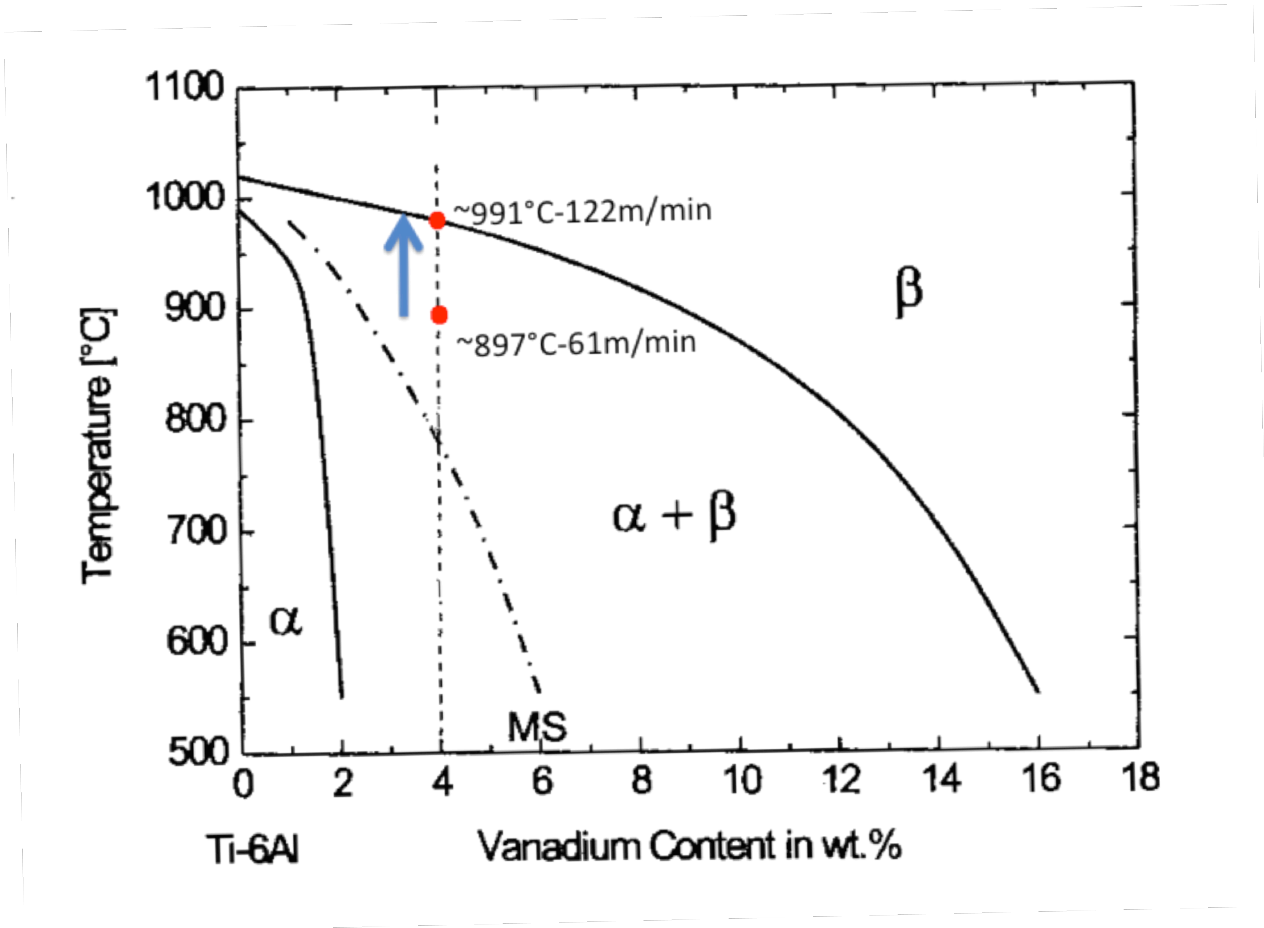

Figure 27: Equilibrium phase diagram for the Ti-6Al - V system showing the 4% V composition line. The point at 897°C corresponds to the temperature for cutting with the PCD insert at 61m/min. The point at 991°C corresponds to the temperature for cutting with the PCD insert at 122m/min.

It is interesting to compare the predicted relative alloy phase fraction for the Ti-64 at the different cutting temperatures predicted by FEM for each cutting speed. Using the inverse lever rule, the relative composition of the titanium chip for the low cutting speed (~897 °C) was expected to be more alpha phase than beta. For higher cutting speeds, the relative amount of beta phase would be expected to increase non-linearly from the phase diagram. At the high cutting speed of 122m/min (~991°C), the phase transformation to beta would be nearly complete. One additional complication for predicting phase change during machining is an effect of high pressure. Mei et al [26] investigated the effect of pressure on phase change in titanium by comparing Young and Debye+Electron models. In both cases, the effect of increased pressure was a decrease in the beta transus temperature with respect to atmospheric pressure. The results of their study are shown in Figure 28. Therefore, additional pressure during machining may have increased the likelihood of a phase change from alpha to beta during chip formation.

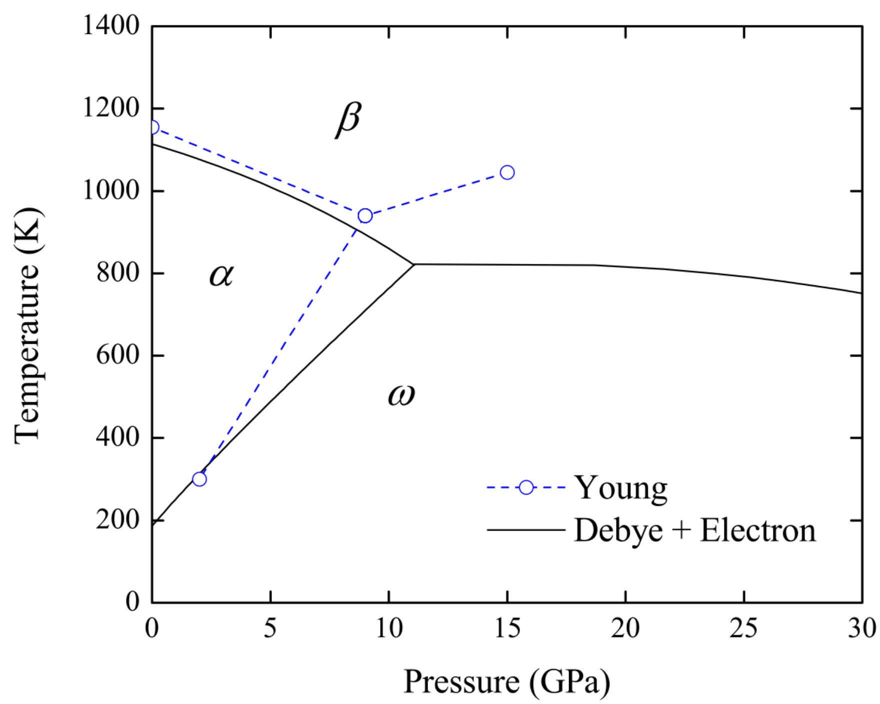

Figure 28: T-P phase diagram for Ti6Al4V [26]

One possible problem with using equilibrium phase diagrams is that phase change is a kinetic process. Any phase change occurring during machining would be occurring at relatively high strain-rates and over short periods of time. These uncertainties demand additional evidence before any phase dependent tool-wear theories can be proposed. This additional evidence can come from study of the microstructure of both the work material and the chip.

Looking at the partitioned OIM scan of the microstructure of the work material in Figure 21, it is clear that a substantial fraction of the scanned area showed grains oriented with basal planes within 30 degrees of the -1 -1 1 direction. This orientation would be highly favorable for basal plane {0001} slip in the <11$\bar{2}$0}> slip direction [25]. This basal slip would promote rapid shear transformation from alpha to beta phase where {0001} alpha planes become {110} planes of the beta phase [25].

The OIM scan of the microstructure of the chip shows direct evidence of phase change. Specifically, there are regions of oscillating 90° misorientations in Figure 22 and Figure 24, which occur near the interface between chip and rake surface but between shear bands. These regions are most likely to be at the highest temperature but less deformed, retaining original microstructure. Upon cooling, variant selection takes place in the prior beta leading to specific, different alpha orientations that are true children of the beta->alpha transformation. These oscillations are not seen in the chip further from the cutting edge. This confirms the likelihood that significant portions of the chip near the chip-tool interface were in the beta phase during machining.

Having established a strong likelihood of phase change during machining of Ti-64 at high cutting speeds using PCD tools and at all cutting speeds using carbide tools, the following discussion will turn to the impact of phase change on the tool wear. It is the difference in the characteristics of the alpha and beta phase that may have played such an important role in determining which wear mechanism dominated. For instance, the self-diffusion coefficient of the beta phase at 1000°C is approximately five orders of magnitude greater that that of alpha phase at 500°C [25]. Such a large increase in movement within the work material may promote diffusion of the constituent atoms of the tool material into the chip. This was supported by the relatively large craters seen on the rake face of the PCD tools cutting at the high cutting speed after only 2 min, whereas no discernable dissolution wear was present on the inserts cutting at the low cutting speed after 24min. As previously stated, the small difference in temperature indicated that no significant difference in diffusion/dissolution wear should be present given similar crystalline structure. Yet there is a huge difference in the observed wear pattern.

A phase change also has the potential to explain the uneven, fractured wear at the low cutting speed. The key to explaining the low speed wear may lie in the difference in plastic deformation characteristics between the alpha and beta phases. To understand the plastic deformation mechanisms, the slip systems of the respective phases of the titanium work material must be understood.

An HCP structure has only 1 slip plane and 3 slip directions [25]. In addition, the alpha phase of titanium is not quite HCP, giving one additional slip plane with 3 slip directions [25]. These slip planes and slip directions give a total of 4 possible independent slip systems [25]. The BCC structure of the beta phase has 6 slip planes in 2 slip directions, for a total of 12 slip systems [25]. Taking packing density and minimum slip length into account, the beta structure is typically much easier to deform as a polycrystalline metal than the alpha phase [25]. Upon chip seizure, the favorable deformation characteristics of beta phase would promote stability of the adhered layer, with chip flow occurring due to internal shear in the chip. On the other hand, alpha phase would resist internal shear, allowing shear stress at the tool-chip interface to build up. This stress may have cause the periodic breaking off of the adhered layer, causing the attrition wear, similar to that identified by adhesion experiments of Nabhani [9]. The difference in the amount of titanium adhered on the tool after machining supports this theory. Figure 18 shows that relatively little titanium remains attached to the rake surface of the PCD tool after machining at 61m/min, while a substantial amount obscures the observation of the craters that occurred at 122m/min.

Extending the theory of phase change to other tool materials is necessary for generalization. If a phase change in the work material does indeed occur, it should affect wear mechanisms operating on other tool materials too. The consistent wear patterns for the tungsten carbides seen in Figure 17 correlates well with the phase dependent tool wear theory. The attrition wear mechanism did not appear at the low cutting speed. Again, the interpretation of tool wear pattern in relation to the temperature on the rake face provided a clue. The temperature estimate from FEM for the carbide tools at the low cutting speed was already 1095°C [11] as presented in Table 3. This temperature is well above the beta transus line for Ti-64. Therefore, there was likely a high proportion of beta phase in the chip during cutting at 61m/min, similar to that when cutting using a PCD tool at 122m/min. Using the same arguments presented for the PCD tools at 122m/min, the transformation to a much higher fraction of beta phase would have promoted diffusion wear for the carbide tools at only 61m/min cutting speed.

CONCLUSION

The results of this study have provided three-dimensional wear data for WC-6Co and PCD inserts turning Ti-6Al-4V. This information will be valuable for the development of future physics-based models that will be able to accurately predict crater wear in the machining of titanium. The crater wear profiles of two grades of WC-6Co have also been analyzed. It was found that the YD201 straight grade inserts with a coarser grain size exhibited less crater wear than that of the YD101 grade with the finer grain size. This was mainly attributed to a difference in thermal conductivity due to grain size. The difference in temperature from the difference in thermal conductivity was confirmed using an FEM. Flank-wear analysis of the carbide tools showed that the finer grain size of WC-6Co was less susceptible to flank wear than the larger grain size. PCD experiments were also conducted. The results demonstrated the superiority of PCD tools for cutting Ti6Al4V. Two different, simultaneously occurring, wear mechanisms were identified. At the low cutting speed, adhesion wear created a scalloped wear profile, whereas dissolution/diffusion predominated at the higher cutting speed.

A new theory has been presented that connects cutting temperature to phase change of Ti-64, explaining differences in observed wear on the rake face of both PCD and carbide inserts. It is believed that phase change from alpha to beta phase causes a transition from attrition wear to dissolution wear in PCD tools. This explains the relatively large spread in wear mechanisms found in the literature. However, carbides tools exhibit dissolution wear at much lower speeds, as cutting temperature is higher and phase change from alpha to beta phase has already occurred.

The results indicate the likelihood of phase change occurring for both cutting speeds during machining of the Ti with the PCD tools are surprising. However, it can be seen from the OIM maps of the microstructure of the chips that more recrystallization occurred during machining at 122m/min. A higher degree of recrystallization provides additional evidence of more self-diffusion within the microstructure of the Ti-64 during machining at 122m/min. The increase in self-diffusion within the microstructure increases defects that allow a higher rate of diffusion wear from the tool material. However, more evidence is needed before connection between the extent of recrystallization and tool wear can be made.

Areas of further research might include investigating the correlation between recrystallization of the microstructure and the tool wear. Furthermore, to improve machinability of titanium, it may be possible to add alloying elements to the carbide tool material to increase the beta transition temperature of the work material in the seizure zone. These additives would be similar to additives such as TiC and TaC, which are common in carbides used to cut steel and other ferrous materials.

Longer term, it may be possible to develop comprehensive tool wear models using FEM or other numerical techniques. These models would use physically based information such as work material phase and grain orientation to calculate mass transfer and stress on the cutting tool.

Finally, the goal of this work was to study tool wear. However, the phase change of the Ti work material may also play important roles in other machining issues such as surface finish of the work piece.

REFERENCES

REFERENCES

[1] A.R. Machado and J. Wallbank, "Machining to Titanium and Its Alloys: A Review," *Proceedings of the Institution of Mechanical Engineers, Part B: Journal of Engineering Manufacture*, vol. 204, pp. 53-60, 1990.

[2] M. Rahman, Zhi-Gang Wang, and Yoke-San Wong, "A Review of High Speed Machining of Titanium Alloys," *Japan Society Mechanical Engineering International Journal, Series C*, vol. 49, no. 1, pp. 11-20, 2006.

[3] P.D. Hartung and B.M. Kramer, "Tool Wear in Titanium Machining," *Ann. CIRP*, vol. 31, no. 1, pp. 75-80, 1982.

[4] J. Hua and R. Shivpuri, "A Cobalt Diffusion Based Model for Predicting Crater Wear of Carbide Tools in Machining Titanium Alloys," in *Transactions of the ASME*, vol. 127, 2005, pp. 136-144.

[5] J. Olortegui-Yume and P. Kwon, "Tool Wear Mechanisms in Machining," *International Journal of Machining and Machinability of Materials*, vol. 2, no. 3/4, pp. 316-334, 2007.

[6] M.P. Groover, *Fudementals of Modern Manufacturing: Materials, Processes, and Systems*, 3rd ed.: John Wiley & Sons, Inc, 2007.

[7] W. Konig and A. Neises, "Wear Mechanisms of Ultrahard, Non-metallic Cutting Materials," *Wear*, vol. 162-164, pp. 12-21, 1993.

[8] N. Corduan, T. Himbert, G. Poulachon, and et. al., "Wear Mechanisms of New Tool Materials for Ti6Al4V High Performance Machining," *CIRP Annals - Manufacturing Technology*, vol. 52, no. 1, pp. 73-76, 2003.

[9] F Nabhani, "Wear Mechisms of Ultra-hard Cutting Tool Materials," *J. Mat. Proc. Tech.*, vol. 115, pp. 402-412, 2001.

[10] M. Wang and Y. Zhang, "Diffusion Wear in Milling Titanium," *Materials Science and Technology*, vol. 4, pp. 548-553, 1988.

[11] D. Schrock, X. Wang, and P. Kwon, "An Analysis of the Wear of Tungsten Carbide and Polycrystalline Diamon Inserts Turning Ti-6Al-4V," in *ASME Conf. Proc.*, vol. 197, 2011.

[12] Z. Z. Fang, "Correlation of Transverse Rupture Strength of WC-Co with Hardness," *International Journal of Refractory Metals & Hard Materials*, vol. 23, pp. 119-127, 2005.

[13] A. Lammer, "Mechanical Properties of Polycrystalline Diamonds," The Institute for Metals, 1988.

[14] R. Shivpuri, J. Hua, P. Mittal, and et. al., "Microstructure-mechanics Interactions in Modeling Chip Segmentation During Titanium Machining," *CIRP Annals - Manufacturing Technology*, vol. 51, no. 1, pp. 71-74, 2002.

[15] P.A. Dearnley and A.N. Grearson, "Evaluation of Principle Wear Mechanims of Cemented Carbides and Ceramics Used for Machining Titanium Alloy IMI 318," *Material Science and Technology*, vol. 2, pp. 47-58, 1986.

[16] J.A. Olortegui-Yume and P.Y. Kwon, "Crater Wear Pattern Analysis on Multi-layer Coated Carbides Using the Wavelet Transform," *Wear*, vol. 268, pp. 493-504, 2010.

[17] EDAX/AMETEK, Inc., Introduction to Orientation Imaging Microscopy.

[18] EDAX-TSL, Software V5.31 User Manual.

[19] H.W. Meyer Jr. and D.S. Kleponis, "An Analysis of Parameters for the Johnson-Cook Model for 2-inch Thick Rolled Homogenous Armor," in *Advanced Simulation Technologies Conference, Military, Government, and Aerospace Simulation Series*, vol. 30, 1998.

[20] W.S. Lee and C.F. Lin, "High-temperature Deformation Behavior of Ti6Al4V Alloy Evaluated by High Strain Rate Compression Tests," *J Mater Process Technol*, vol. 75, no. 1-3, pp. 127-136, 1998.

[21] H.W. Meyer Jr. and D.S. Kleponis, "Modeling the High Strain Rate Behavior of Titanium Undergoing Ballistic Impact and Penetration," *Int J Impact Eng*, vol. 26, no. 1-10, pp. 509-521, 2001.

[22] Z.G. Wang, M. Rahman, Y.S. Wong, and X.P. Li, "A Hybrid Cutting Force Model for High-speed Milling of Titanium Alloys," *CIRP Annals - Manufacturing Technology*, vol. 54, no. 1, 2005.

[23] E.M. Trent and P.K. Wright, *Metal Cutting*.: Butterworth-Heinemann, 2000.

[24] M.V. Frandsen, Ph.D Dissertaion, The University of Illinois, 1987.

[25] C. Leyens and M. Peters, *Titanium and Titanium Alloys: Fundementals and Applications*. Weinheim, Germany: Wiley-VCH Verlag GmbH & Co. KGaA, 2003.

[26] Z. Mei, S. Shang, Y. Wang, and Z. Liu, "Density-functional Study of the Thermodynamic Properties and the Pressure-temperature Phase Diagram of Ti," *Physical Review B*, vol. 80, no. 104116, 2009.